Published November 8, 2010

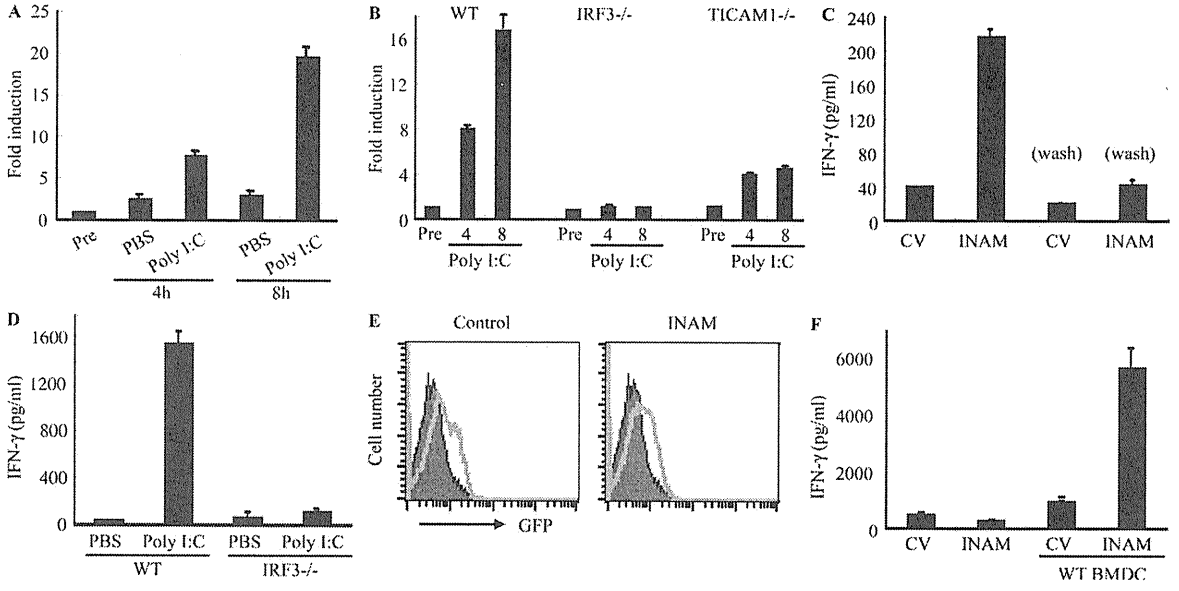

Figure 6. INAM on NK cells contributes to efficient NK activation mediated by mDC. (A and B) Quantitative RT-PCR for INAM expression in WT, TICAM1$^{-/-}$, or IRF-3$^{-/-}$ NK cells stimulated with 50 µg/ml polyI:C. Data shown are means of duplicate or triplicate samples from one experiment that is representative of three. (C) IRF-3$^{-/-}$ BMDCs were transfected with control lentivirus (CV) or INAM-expressing lentivirus (INAM) before treatment with 10 µg/ml polyI:C for 4 h. BMDCs in some wells were washed to remove polyI:C before WT NK cells were added (Wash). IFN-γ production by NK cells was determined by ELISA after 24 h of culture. Data show one of two similar experimental results. (D) ELISA of IFN-γ in co-culture of WT or IRF-3$^{-/-}$ NK cells and WT BMDC with/without 10 µg/ml polyI:C. (E and F) NK cells were transfected with control lentivirus or INAM-expressing lentivirus and cultured with 500 IU/ml IL-2 for 3 d. After determining transfection efficiency by GFP intensity using flow cytometry, cells were cultured with/without BMDC for 24 h and IFN-γ production in the supernatant determined by ELISA. Shaded peak, noninfected control; open peak, infected BMDC. All data are means ± SD of triplicate samples from one experiment that is representative of three.

we washed polyI:C out and cultured the cells with WT NK cells (Fig. 6 C, right two lanes). Under these conditions, in which polyI:C acted not on NK cells but only on BMDC, little NK activation was observed (Fig. 6 C). Furthermore, IRF-3$^{-/-}$ NK cells produced little IFN-γ when co-cultured with WT BMDC and polyI:C (Fig. 6 D). INAM-overexpressing IRF-3$^{-/-}$ BMDC required IRF-3 in NK cells for efficient BMDC-mediated production of IFN-γ from NK cells (Fig. 6 D). We next transduced INAM into IRF-3$^{-/-}$ NK cells using a lentivirus (INAM/pLenti-IRES-hrGFP) to reconstitute NK IFN-γ–producing activity. After many trials with various setting conditions, we found that ~15% of the DX5^{+} NK cell population was both GFP-positive and stained with anti-FLAG mAb when treated with high doses of INAM-expressing lentivirus vector (Fig. S7 B). When IRF-3$^{-/-}$ NK cells were infected with smaller amounts of INAM-expressing lentiviral vector and cultured for 3 d with high concentrations of IL-2 (500 IU/ml), slight but significant GFP expression was confirmed by FACS (Fig. 6 E). Then, the INAM-transduced IRF-3$^{-/-}$ NK cells were co-cultured with WT BMDC. The IRF-3$^{-/-}$ NK cells with INAM expression secreted IFN-γ at significantly higher levels than controls in the presence of WT BMDC (Fig. 6 F). These data indicate that INAM is induced by polyI:C through IRF-3 activation, not only in BMDCs but also in NK cells, and that INAM on NK cells synergistically works with INAM on BMDC for efficient NK cell activation. Both INAMs on BMDC and NK cells are essential for BMDC-mediated NK activation.

We next checked the function of the C-terminal stretch of INAM in NK activation. Although intact INAM works in NK cells to produce IFN-γ in response to BMDC (Fig. 6 F), introduction of C-del INAM into IRF-3$^{-/-}$ NK cells did not result in high induction of IFN-γ in response to BMDC (Fig. 4 C). Thus, INAM participates in NK activation through its cytoplasmic regions, which has no significant role in BMDC for NK activation.

Anti-tumor NK activation via INAM-expressing BMDCs in vivo

mDC-mediated NK activation induces anti-tumor NK cells, which cause regression of NK-sensitive tumors (Kalinski et al., 2005; Akazawa et al., 2007a). We tested the in vivo function of INAM-expressing BMDC using B16D8 tumor-bearing mice. BMDCs were used 24 h after transfection with either INAM/pLenti-IRES-hrGFP or control pLenti-IRES-hrGFP and injected twice a week s.c. around a preexisting tumor in tumor-implanted mice, beginning 11–13 d after tumor challenge. INAM-expressing BMDC significantly retarded tumor growth (Fig. 7 A). Tumor retardation was abrogated by depletion of NK1.1-positive cells (Fig. 7 B). Thus, INAM expression on BMDC contributed to anti-tumor NK activation in vivo.

When the control or INAM-expressing IRF-3$^{-/-}$ BMDCs were co-cultured with WT NK cells in vitro, there was no induction of the mRNA of TRAIL and granzyme B in

Published November 8, 2010

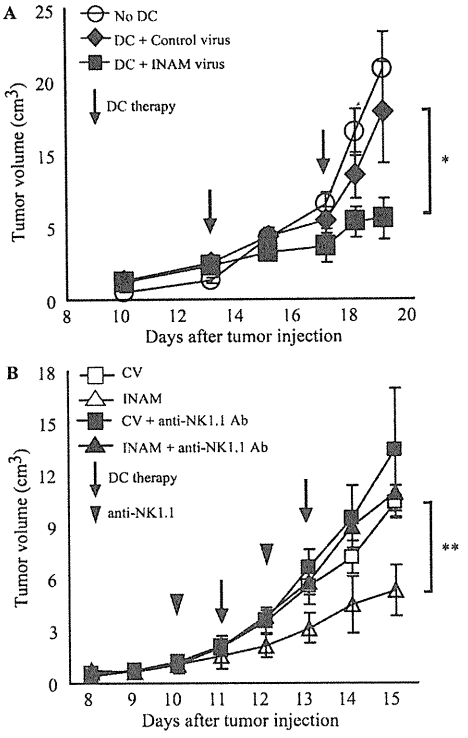

Figure 7. INAM on BMDC retarded B16D8 tumor growth in an NK-dependent manner. (A) Tumor volume after DC therapy using BMDC expressing INAM. B16D8 cells were s.c. injected into C57BL/6 mice and, 11–13 d later, medium only (○) or BMDC (10^6/mouse) transfected with control lentivirus (◆) or those with INAM-expressing lentivirus (■) were administered s.c. near the tumor at the time indicated by the open arrow. *, P = 0.043. Data represent mean ± SD. (B) Abrogation of INAM-dependent tumor regression by administration of NK1.1 Ab. For depletion of NK cells, antiNK1.1 mAb was injected i.p. 1 d before treatment of BMDC (arrowheads). Tumor volume in every mouse group was sequentially monitored. Data represent mean ± SD (n = 3) and are representative of two experiments. Statistical analyses were made with the Student's t test. **, P = 0.017.

NK cells (Fig. 8 A). TRAIL and granzyme B were induced in NK cells by the addition of polyI:C to the mixture, and INAM expression in BMDC up-regulated mRNA levels of TRAIL and granzyme B (Fig. 8 A). In vivo administration studies were performed with polyI:C-treated WT BMDC or INAM-expressing IRF-$3^{-/-}$ BMDC to test their ability to up-regulate the mRNA levels of TRAIL and granzyme B in NK cells in draining LN (Fig. 8 B). INAM-expressing IRF-$3^{-/-}$ BMDC showed comparable abilities to up-regulate the killing effectors with polyI:C-treated BMDC (Fig. 8 B). Collectively, INAM has therapeutic potential for NK-sensitive tumors by activating NK cells.

DISCUSSION

Previous studies demonstrated that mDC–NK interaction leads to direct NK activation and damages NK target cells in vitro (Gerosa et al., 2002; Sivori et al., 2004; Akazawa et al., 2007a; Lucas et al., 2007). In addition, mDCs initiate NK cell–mediated innate anti-tumor immune responses in vivo (Kalinski et al., 2005; Akazawa et al., 2007a,b). Systemic administration of polyI:C unequivocally results in activation of peripheral NK cells (Lee et al., 1990; Sivori et al., 2004; Akazawa et al., 2007a). Although the molecular mechanism by which mDCs prime NK cells was still unclear, the TICAM-1 pathway and IPS-1 pathway have been reported to participate in polyI:C-mediated mDC maturation that drives NK activation (Akazawa et al., 2007a; McCartney et al., 2009; Miyake et al., 2009). We have shown in an earlier study that mDCs disrupted in the TLR3–TICAM-1 pathway abrogate NK cell activation (Akazawa et al., 2007a,b). In TICAM-$1^{-/-}$ mice, NK-sensitive implant tumors grew as well as those in WT mice depleted of NK cells (Akazawa et al., 2007a). mDCs gain high anti-tumor potential against B16D8 implant tumors through lentiviral transfer of TICAM-1, which is attributable to NK activation (Akazawa et al., 2007a). We further showed that TICAM-1 is a critical molecule for mDC to induce NK cell IFN-γ, as well as IPS-1, and participates in driving NK cytotoxicity to a lesser extent than IPS-1. In this paper, we clarified a molecular mechanism by which mDCs immediately promote NK cell functions in vitro and in vivo.

Our findings showed that IRF-3 is the transcription factor that is downstream of TICAM-1 responsible for maturing mDC to an NK-activating phenotype. We discovered that INAM, a membrane-associated protein, is up-regulated on the surface of mDC by polyI:C stimulation and activates NK cells via cell–cell contact. Furthermore, we found that NK cells also express INAM on their cell surface after polyI:C stimulation. mDC–NK activation by polyI:C can be reproduced with INAM-transduced mDC and NK cells, and adoptive transfer experiments show that INAM-overexpressing mDC may have therapeutic potential against MHC-low melanoma cells in an NK-dependent manner. These functional properties of INAM-expressing mDC fit the model of mDC priming NK activation. Ultimately, INAM appears to be the key molecule in the previously reported mechanism of mDC–NK contact activation.

After the submission of this manuscript, two papers were published that found that the MDA5–IPS-1 pathway in mDC is more important for driving NK activation, particularly in vivo (McCartney et al., 2009; Miyake et al., 2009). Our data also support this point using the IPS-$1^{-/-}$ mice we established (Fig. S1). However, polyI:C, when i.v. administered into mice, may stimulate other systemic cells in addition to $CD8^+$ mDC in vivo (McCartney et al., 2009). The difference among the two (McCartney et al., 2009; Miyake et al., 2009) and this study may be attributed to the setting conditions, which are not always comparable. Moreover, it remains to be settled whether TICAM-1 and IPS-1 take the same INAM complex as a common NK activator in mature mDC and whether TLR3 (or MDA5) KO is equivalent to TICAM-1 (or IPS-1) KO in the mDC–NK activation model. In either case, however, up-regulation of mDC TICAM-1–mediated NK cytotoxicity and IFN-γ induction are feasible with polyI:C under three different conditions (Akazawa et al., 2007a; McCartney et al., 2009; Miyake et al., 2009). Our results infer that INAM participates in at least these mDC–NK interactions.

Published November 8, 2010

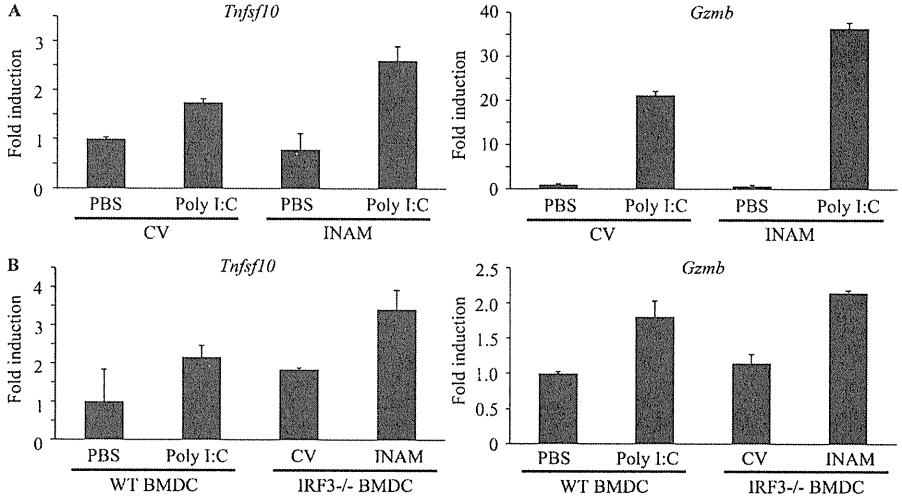

Figure 8. INAM-mediated induction of TRAIL and granzyme B in BMDC. (A) In vitro induction of TRAIL (Tnfsf10) and granzyme B (Gzmb) mRNA by INAM-expressing BMDC. BMDCs (IRF-3$^{-/-}$) were infected with INAM-expressing virus or CV as in Fig. S4. After 24 h, the BMDCs (IRF-3$^{-/-}$) were incubated with WT NK cells at DC/NK = 1:2. 8 h later, DX5^{+} cells were collected by FACS sorting and their RNA was extracted to determine the mRNA levels of the indicated genes. A representative result of three similar experiments are shown. (B) In vivo induction of TRAIL and granzyme B mRNA by INAM-expressing BMDC. WT BMDCs were stimulated with 10 μg/ml polyI:C or medium only. IRF-3$^{-/-}$ BMDCs were infected with CV or INAM-expressing vector. These BMDCs were allowed to stand for 24 h and then 5 × 10^{5} cells were injected into footpads of WT mice. After 48 h, DX5^{+} cells were collected from the inguinal LN by FACS sorting. RNA of the cells was extracted and the levels of the indicated mRNA were determined by real time PCR. Data show one of two experiments with similar results. Data in A and B represent mean ± SD.

PolyI:C activates IRF-3 through the two pathways involving the adaptors IPS-1 and TICAM-1 (Yoneyama et al., 2004; Kato et al., 2006; Matsumoto and Seya, 2008). The two pathways share the complex of IRF-3–activating kinase, NAP1, IKK-ε, and TBK1 that is downstream of adaptors (Sasai et al., 2006). Nevertheless, these pathways are capable of inducing several genes unique to each adaptor. Although IFN-α production by in vivo administration of polyI:C is largely dependent on the IPS-1 pathway, IL-12p40 is mainly produced by the TICAM-1 pathway (Kato et al., 2006). Therefore, it is not surprising that INAM induction is predominant in the TICAM-1 pathway in polyI:C-stimulated BMDC (Fig. 3 A). What happens in IRF-7$^{-/-}$ BMDCs in terms of INAM induction and what mechanism sustains BMDC IPS-1–mediated or MyD88-mediated activation of NK cells (Azuma et al., 2010) will be issues to be elucidated in the future.

Although IRF-3–regulated cell surface INAMs are required for efficient interaction between BMDC and NK cells, the mechanism by which forced expression of INAM causes signaling for BMDC maturation is still unknown. Although the NK-activating capacity of BMDCs is usually linked to their maturation, neither cytokines in NK activation, including IFN-α and IL-12p70, nor costimulators, such as CD40 and CD86, were specifically induced in mDC by INAM expression (Fig. S5). INAM has a C-terminal cytoplasmic stretch (Fig. 4 A), and we tested the function of this region by a deletion mutant (C-del INAM). This region in BMDC barely participates in driving NK activation because no decrease of IFN-γ induction by NK cells was observed with IRF-3$^{-/-}$ BMDC supplemented with C-del INAM compared with control INAM. Thus far, no significant signal alteration has been detected in BMDC supplemented with INAM by lentivirus.

In contrast, INAM-transduced IRF-3$^{-/-}$ NK cells produced IFN-γ in concert with BMDCs like WT NK cells (Fig. 6 F). So far we have no evidence suggesting that this kind of INAM overexpression is actually occurring in vivo. However, introduction of C-del INAM into IRF-3$^{-/-}$ NK cells did not result in high induction of IFN-γ in response to BMDC (Fig. 4 C). Together with the data on INAM expression in BMDC, this infers that the INAM cytoplasmic region signals for NK activation in NK cells. The one-way role of the cytoplasmic tail in NK activation will be an issue for further analysis.

In this study, IL-15 was found to be up-regulated by polyI:C in BMDC. The remaining NK activity in the resting population of NK cells co-cultured with TICAM-1$^{-/-}$ BMDC and polyI:C (Fig. 1 B) suggests that IL-15 has some effect in our system, and other studies suggest this as well (Ohteki et al., 2006; Brilot et al., 2007; Lucas et al., 2007; Huntington et al., 2009). However, we did not observe decreased IL-15 expression in the TICAM-1$^{-/-}$ BMDC that could not activate NK cells (Fig. 1 E). Several molecules, such as B7-H6/NKp30 (Brandt et al., 2009), CD48/2B4 (Kubin et al., 1999), and NKG2D ligands/NKG2D (Cerwenka et al., 2000), have been identified as ligand/receptor molecules in mDC–NK reciprocal activation by in vitro co-culture. In in vitro co-culture systems (Fig. S1), the IPS-1 pathway in BMDC has a pivotal role in not only type I IFN but also IL-15 induction. INAM identified in this paper serves a unique function in the in vivo induction of NK activation and may offer a tool to investigate the reported mDC-mediated NK activation.

Rae-1 was reported as a molecule with MHC-like structure (Zou et al., 1996) and later identified as a mouse NKG2D ligand (Cerwenka et al., 2000). Although Rae-1 is a GPI-anchored protein with no cytoplasmic sequences (Nomura et al., 1996), it can act as an NK-activating ligand (Cerwenka et al., 2000, 2001; Masuda et al., 2002). Mouse BaF3 cells become NK-sensitive after forced expression of Rae-1α (Masuda et al., 2002). Actually, mouse macrophages induce Rae-1 expression in response to TLR stimuli (Hamerman et al., 2004). In contrast,

Published November 8, 2010

INAM-expressing stable BaF3 cell lines (INAM/BaF3) did not reveal a function as an NK cell–activating ligand. NK cell cytotoxicity is directed against Rae-1α/BaF3 cells but not against INAM/BaF3 cells (Fig. 5). Therefore, INAM does not represent a typical NK cell–activating ligand. For NK activation, INAM on BMDC appears to require other molecules that are expressed in BMDC but not in BaF3.

INAM has four transmembrane regions, similar to the cell adhesion tetraspanins, which may support cell–cell contact (Levy and Shoham, 2005). Tetraspanins provide a scaffold that facilitates complex formation with associated proteins. INAM on BMDC and NK cells may use cell–cell interaction to assemble in a synaptic formation to activate NK cells. Because the protein constituents of the tetraspanin complexes are cell specific, we are interested in finding partners for INAM that might participate in efficient BMDC–NK interaction. TLR-inducible cell–cell contact may occur through INAM in an immune cell–specific manner. Gene disruption of this INAM will facilitate clarifying this issue. The identification of INAM defines a novel pathway in mDC–NK reciprocal interaction. This study will lead to further research on the molecules that form complexes on BMDC and NK cells to facilitate BMDC–NK interaction.

MATERIALS AND METHODS

Mice. All mice were backcrossed with C57BL/6 mice more then seven times before use. TICAM-1$^{-/-}$ (Akazawa et al., 2007a) and IPS-1$^{-/-}$ mice were generated in our laboratory. IRF-3$^{-/-}$ (Sato et al., 2000) and IRF-7$^{-/-}$ mice (Honda et al., 2005) were provided by T. Taniguchi (University of Tokyo, Tokyo, Japan). All mice were maintained under specific pathogen-free conditions in the animal facility of the Hokkaido University Graduate School of Medicine. Animal experiments protocols and guidelines were approved by the Animal Safety Center, Hokkaido University, Japan.

Cells. The B16D8 cell line was established in our laboratory as a subline of B16 melanoma (Tanaka et al., 1988). This subline was characterized by its low or virtually no metastatic properties when injected s.c. into syngeneic C57BL/6 mice. B16D8 was cultured in RPMI 1640/10% FCS. The mouse B cell line BaF3 was obtained from American Type Culture Collection and cultured in RPMI 1640/10% FCS/2 μM 2ME/5 ng/ml IL-3. Mouse NK cells (DX5^{+} cell) were positively isolated with MACS Beads (Miltenyi Biotec). Mouse BMDCs were prepared as previously reported (Akazawa et al., 2007a).

For purification of cells from spleen or LN, these tissues were treated with 400 IU MandleU/ml collagenase D (Roche) at 37°C for 25 min in HBSS (Sigma-Aldrich). Then EDTA was added, and the cell suspension was incubated for an additional 5 min at 37°C. After removal of RBC with ACK lysis buffer, splenocytes and LN cells were stained with CD45-FITC, CD3ε-PE, CD19-PE, DX5-PE, CD11b-FITC (eBioscience), and CD11c-FITC (BioLegend) and sorted by a FACSAria II (BD). The purity of sorted cells were >96%.

Construction and expression. Mouse INAM cDNA (A630077B13Rik) was obtained from RIKEN and placed into expression vector pEFBOS and pLenti-IRES-hrGFP, both of which provide the specialized components needed for expression of a recombinant C-terminal FLAG fusion (Akazawa et al., 2007a). For construction of shRNA-expressing lentivirus vector, The ClaI–XhoI fragment of pLenti6-blockit-dest (Invitrogen) was inserted into pLenti-IRES-hrGFP at the site of ClaI and XhoI. This vector was named pLenti-dest-IRES-hrGFP (pLDIG). INAM sequence 5′-CTTCTCTCCG-GTTAGTTATCT-3′ was targeted for INAM knockdown (shINAM/pLDIG) and 5′-AGTCTGACATACTTATACTTA-3′ was used for negative control (shCont/pLDIG). We used a gene-expression kit, Lentiviral system (Invitrogen), as previously described (Akazawa et al., 2007a). Four plasmids (one of the pLenti vectors, pLP1, pLP2, and pLP/VSVG) were transfected into 293 FT packaging cells, and the viral particles for transfection were prepared according to the manufacturer's protocol. The 100× concentrated virus particles were produced after centrifugation of 8,000 *g* at 4°C for 16 h. Lentivirus produced by pLenti-IRES-hrGFP and pLDIBG could be tittered by GFP expression using flow cytometry. Because the lentivirus vector pLenti-IRES-hrGFP has the IRES-GFP region, we prepared negative control virus by pLenti-IRES-hrGFP without construct. Infection efficiency for BMDC was high with the control vector compared with the INAM-expressing lentivector (Fig. S6 A).

Real-time PCR. BMDCs were harvested after 4 h of stimulation by 100 ng/ml LPS, 50 μg/ml polyI:C, 1 μg/ml Pam_3CSK_4 (Pam3), 100 nM mycoplasmal macrophage-activating lipopeptide-2 (Malp-2), 10 μg/ml CpG, and 2,000 IU/ml IFN-α (Ebihara et al., 2007). Mouse tissues (heart, stomach, small intestine, large intestine, lung, brain, muscle, liver, kidney, thymus, and spleen) were collected from C57BL/6. Splenocytes were stained with CD3-PE, CD19-PE, DX5-PE, CD11b-PE, CD11c-FITC, and PDCA1-PE (eBioscience) and sorted by FACSAria (BD). Purity was >98% in each population. For RNA extraction, we used the RNeasy kit (Invitrogen). After removal of genomic DNA by treatment with DNase, randomly primed cDNA strands were generated with Moloney mouse leukemia virus reverse transcription (Promega). RNA expression was quantified by quantitative RT-PCR with gene-specific primers (IL-15 forward, 5′-TTAACTGAGGCTGGCATTCATG-3′; IL-15 reverse, 5′-ACCTACACTGACACAGCCCAAA-3′; INAM forward, 5′-CAACTGCAATGCCACGCTA-3′; INAM reverse, 5′-TCCAACC-GAACACCTGAGACT-3′; β-actin forward, 5′-TTTGCAGCTCCTTC-GTTGC-3′; β-actin reverse, 5′-TCGTCATCCATGGCGAACT-3′; HPRT forward, 5′-GTTGGATACAGGCCAGACTTTGTTG-3′; and HPRT reverse, 5′-GAAGGGTAGGCTGGCCTATAGGCT-3′) and values were normalized to the expression of β-actin mRNA or HPRT mRNA.

Other primers for PCR were designed using Primer Express software (Applied Biosystems) for another experiment. The following primers were used for PCR: β-actin forward, 5′-CCTGGCACCCAGCACAAT-3′ and reverse, 5′-GCCGATCCACACGGAGTACT-3′; granzyme B forward, 5′-TCCTGCTACTGCTGACCTTGTC-3′ and reverse, 5′-ATGATCTC-CCCTGCCTTTGTC-3′; IFN-α4 forward, 5′-CTGCTGGCTGTGAG-GACATACT-3′ and reverse, 5′-AGGCACAGAGGCTGTGTTTCTT-3′; TRAIL (Tnfsf10) forward, 5′-CTTCACCAACGAGATGAAGCAG-3′ and reverse, 5′-TCCGTCTTTGAGAAGCAAGCTA-3′; and IL-12p40 (Il12b), forward, 5′-AATGTCTGCGTGCAAGCTCA-3′ and reverse, 5′-ATGCCCACTTGCTGCATGA-3′.

Anti-INAM pAb. C-terminal INAM (cINAM; 191–314 aa) was subcloned between the NdeI and SalI sites of pColdI vector (Takara Bio Inc.). 6× His-tagged cINAM protein was expressed in BL21 by manufacturer's methods. The cells were sonicated in 20 mM Tris-HCl, 150 mM NaCL, 1 mM PMSF, and 7 M Urea, pH 7.4, on ice. Expression products of cINAM were purified using the HisTrap HP kit (GE Healthcare). The extracted proteins were refolded by stepwise dialysis against decreasing amounts of urea. Rabbit anti-cINAM polyclonal Ab was produced with the cINAM proteins by standard protocol. IgG was purified by precipitation with 33% ammonium sulfate, dialyzed against PBS.

Surface labeling with biotin. Biotinylation of cell surface proteins was performed according to the reported method (Tsuji et al., 2001). In brief, ~10^8 cells were suspended in 1 ml Hepes-buffered saline (HBS), pH 8.5, and incubated with 10 ml of 10 mg/ml NHS-sulfobiotin (Vector Laboratories) for 1 h at room temperature. Cells were washed in HBS three times and then solubilized with lysis buffer containing 1% NP-40, pH 7.4. The cell lysate was immunoprecipitated with avidin-labeled Abs as described previously (Tsuji et al., 2001).

Immunoblot analysis. Lysates were harvested 24 h after transfection of Flag-tagged INAM/pEFBOS into 293FT cells and treated with *N*-glycosidase F

(PNGaseF; New England Biolabs, Inc.) by the manufacturer's method in some experiments. Protein samples were separated on SDS-PAGE and immunoblotted by anti-Flag M2 Ab (Sigma-Aldrich). In some experiments, we used highly purified rabbit anti–mouse INAM polyclonal Ab for immunoblotting. The anti-INAM IgG was further purified with protein A–Sepharose and absorbed with BL21 bacterial lysate (where the INAM immunogen was produced) that contained no INAM peptide.

Confocal microscopy. BMDCs and NK cells were infected with control or INAM-expressing lentivirus as described previously (Akazawa et al., 2007a). 24 h later, cells were fixed with 4% paraformaldehyde for 30 min and permeabilized with PBS containing 0.5% saponin for 30 min at room temperature. Fixed cells were stained with anti-FLAG mAb and Alexa Fluor 568–conjugated secondary Ab. Stable Ba/F3 transfectants expressing INAM were treated with Cytofix/Cytoperm (BD) according to the manufacturer. Then cells were stained with PE-phalloidin and rabbit anti-INAM pAb followed by Alexa Fluor 488–conjugated secondary Ab. Cells were analyzed on a confocal microscope (LSM 510 META; Carl Zeiss, Inc.) for the detection of INAM.

BMDC–NK interaction. BMDCs were co-cultured with freshly isolated NK cells (BMDC/NK = ~1:2–1:5) with or without 10 μg/ml polyI:C for 24 h (Akazawa et al., 2007a). In some experiments, function of BMDCs and NK cells was modified by lentivirus vector before BMDC/NK co-culture. IRF-3$^{-/-}$ BMDCs were transfected by control lentivirus and INAM-expressing lentivirus (INAM/pLenti-IRES-hrGFP) and incubated with 6 μg/ml polybrene for 24 h before co-culture. WT BMDCs were transfected with shRNA-expressing lentivirus (shCont/pLDIG or shINAM/pLDIG) and incubated with 6 μg/ml polybrene for 48 h before co-culture. Freshly isolated NK cells were transfected with control lentivirus and INAM-expressing lentivirus (INAM/pLenti-IRES-hrGFP) and cultured with 6 μg/ml polybrene in the presence of 500 IU/ml IL-2 for 72 h before co-culture. Activation of NK cells was assessed by concentration of IFN-γ (ELISA; GE Healthcare) in the medium and by NK cytotoxicity against B16D8. Cytotoxicity was determined by standard ^{51}Cr release assay as described previously (Akazawa et al., 2007a).

Ex vivo NK activation. Mice were i.p. injected with 250 μg polyI:C. After 24 h, spleen cells were harvested and then NK cells (DX5$^+$ cells) were positively isolated with the MACS system (Miltenyi Biotec). The DX5$^+$ NK cells were suspended in RPMI1640 with 10% FCS and mixed with ^{51}Cr-labeled B16D8 cells at indicated E/T ratios. After 4 h, supernatants were harvested and ^{51}Cr release was measured. Specific lysis was calculated by (specific release − spontaneous release)/(max release − spontaneous release). In some experiments, blood was drawn from the eyes of mice 8 h after polyI:C administration for cytokine measurement.

Test for in vivo NK activation in LN. 5 × 10^5 WT BMDCs incubated with or without 10 μg/ml polyI:C for 24 h or 5 × 10^5 IRF-3$^{-/-}$ BMDCs infected with control virus or INAM-expressing lentivirus and allowed to stand for 24 h were injected into the footpads of WT C57BL/6 mice. 48 h later, cells in their inguinal LN were harvested, stained with PE-DX5, and sorted by FACSAria II. RNA was extracted from the DX5-positive cells with TRIzol.

DC therapy. DC therapy against mice with B16D8 tumor burden was described previously (Akazawa et al., 2007a). C57BL/6 mice (n = 3) were shaved at the flank and injected s.c. with 6 × 10^5 syngeneic B16D8 melanoma cells (indicated as day 0). For DC therapy, BMDCs were prepared by transfecting control lentivirus or INAM-expressing lentivirus (INAM/pLenti-IRES-hrGFP) and cultured for 24 h. At the time point indicated in the figures, 10^6 BMDCs were injected s.c. near the tumor. To deplete NK cells in vivo, mice were i.p. injected with hybridoma ascites of anti-NK1.1 mAb (PK136; Akazawa et al., 2007a). Tumor volumes were measured using a caliper every 1 or 2 d. Tumor volume was calculated using the formula: tumor volume (cm^3) = (long diameter) × (short diameter) × (short diameter) × 0.4.

Statistical analysis. Statistical analyses were made with the Student's t test. The p-value of significant differences is reported.

Online supplemental material. TICAM-1–inducible genes encoding putative membrane proteins relevant for this study are summarized in Table S1. Fig. S1 shows KO mice results suggesting that both IPS-1 and TICAM-1 in BMDC participate in polyI:C-driven NK activation. Data presented in Fig. S2 characterizes the in vivo polyI:C response of INAM in LN cells. Figs. S3 and S4 demonstrate the properties of surface-expressed INAM analyzed by immunoprecipitation/blotting and confocal microscopy, respectively. Fig. S5 mentions the cytokine expression and maturation profiles of INAM-overexpressing BMDC. Fig. S6 shows the effect of gene silencing of INAM on the polyI:C-mediated cytokine-inducing profile in BMDC. Two pieces of data presented in Fig. S7 confirm the presence of the INAM protein in INAM lentivirus-transduced BMDCs and NK cells. Online supplemental material is available at http://www.jem.org/cgi/content/full/jem.20091573/DC1.

We thank Drs. T. Akazawa and N. Inoue (Osaka Medical Center for Cancer, Osaka, Japan) for their valuable discussions. Thanks are also due to many discussions by our laboratory members. Particularly, extensive English review by Dr. Hussein H. Aly is gratefully acknowledged.

This project was supported by Grants-in-Aid from the Ministry of Education, Science, and Culture and the Ministry of Health, Labor, and Welfare of Japan, Mitsubishi Foundation, Mochida Foundation, NorthTec Foundation Waxman Foundation, and Yakult Foundation.

The authors declare no financial or commercial conflict of interest.

Submitted: 20 July 2009
Accepted: 13 October 2010

REFERENCES

Akazawa, T., T. Ebihara, M. Okuno, Y. Okuda, M. Shingai, K. Tsujimura, T. Takahashi, M. Ikawa, M. Okabe, N. Inoue, et al. 2007a. Antitumor NK activation induced by the Toll-like receptor 3-TICAM-1 (TRIF) pathway in myeloid dendritic cells. *Proc. Natl. Acad. Sci. USA.* 104:252–257. doi:10.1073/pnas.0605978104

Akazawa, T., M. Shingai, M. Sasai, T. Ebihara, N. Inoue, M. Matsumoto, and T. Seya. 2007b. Tumor immunotherapy using bone marrow-derived dendritic cells overexpressing Toll-like receptor adaptors. *FEBS Lett.* 581:3334–3340. doi:10.1016/j.febslet.2007.06.019

Azuma, M., R. Sawahata, Y. Akao, T. Ebihara, S. Yamazaki, M. Matsumoto, M. Hashimoto, K. Fukase, Y. Fujimoto, and T. Seya. 2010. The peptide sequence of diacyl lipopeptides determines dendritic cell TLR2-mediated NK activation. *PLoS One.* 5:e12550. doi:10.1371/journal.pone.0012550

Bertram, L., B.M. Schjeide, B. Hooli, K. Mullin, M. Hiltunen, H. Soininen, M. Ingelsson, L. Lannfelt, D. Blacker, and R.E. Tanzi. 2008. No association between CALHM1 and Alzheimer's disease risk. *Cell.* 135:993–994, author reply :994–996. doi:10.1016/j.cell.2008.11.030

Brandt, C.S., M. Baratin, E.C. Yi, J. Kennedy, Z. Gao, B. Fox, B. Haldeman, C.D. Ostrander, T. Kaifu, C. Chabannon, et al. 2009. The B7 family member B7-H6 is a tumor cell ligand for the activating natural killer cell receptor NKp30 in humans. *J. Exp. Med.* 206:1495–1503. doi:10.1084/jem.20090681

Brilot, F., T. Strowig, S.M. Roberts, F. Arrey, and C. Münz. 2007. NK cell survival mediated through the regulatory synapse with human DCs requires IL-15Ralpha. *J. Clin. Invest.* 117:3316–3329. doi:10.1172/JCI31751

Cerwenka, A., and L.L. Lanier. 2001. Natural killer cells, viruses and cancer. *Nat. Rev. Immunol.* 1:41–49. doi:10.1038/35095564

Cerwenka, A., A.B. Bakker, T. McClanahan, J. Wagner, J. Wu, J.H. Phillips, and L.L. Lanier. 2000. Retinoic acid early inducible genes define a ligand family for the activating NKG2D receptor in mice. *Immunity.* 12:721–727. doi:10.1016/S1074-7613(00)80222-8

Cerwenka, A., J.L. Baron, and L.L. Lanier. 2001. Ectopic expression of retinoic acid early inducible-1 gene (RAE-1) permits natural killer cell-mediated rejection of a MHC class I-bearing tumor in vivo. *Proc. Natl. Acad. Sci. USA.* 98:11521–11526. doi:10.1073/pnas.201238598

Dreses-Werringloer, U., J.C. Lambert, V. Vingtdeux, H. Zhao, H. Vais, A. Siebert, A. Jain, J. Koppel, A. Rovelet-Lecrux, D. Hannequin, et al. 2008. A polymorphism in CALHM1 influences Ca2+ homeostasis,

Abeta levels, and Alzheimer's disease risk. *Cell.* 133:1149–1161. doi:10.1016/j.cell.2008.05.048

Ebihara, T., H. Masuda, T. Akazawa, M. Shingai, H. Kikuta, T. Ariga, M. Matsumoto, and T. Seya. 2007. Induction of NKG2D ligands on human dendritic cells by TLR ligand stimulation and RNA virus infection. *Int. Immunol.* 19:1145–1155. doi:10.1093/intimm/dxm073

Fernandez, N.C., A. Lozier, C. Flament, P. Ricciardi-Castagnoli, D. Bellet, M. Suter, M. Perricaudet, T. Tursz, E. Maraskovsky, and L. Zitvogel. 1999. Dendritic cells directly trigger NK cell functions: cross-talk relevant in innate anti-tumor immune responses in vivo. *Nat. Med.* 5:405–411. doi:10.1038/7403

Fitzgerald, K.A., S.M. McWhirter, K.L. Faia, D.C. Rowe, E. Latz, D.T. Golenbock, A.J. Coyle, S.M. Liao, and T. Maniatis. 2003. IKKepsilon and TBK1 are essential components of the IRF3 signaling pathway. *Nat. Immunol.* 4:491–496. doi:10.1038/ni921

Gerosa, F., B. Baldani-Guerra, C. Nisii, V. Marchesini, G. Carra, and G. Trinchieri. 2002. Reciprocal activating interaction between natural killer cells and dendritic cells. *J. Exp. Med.* 195:327–333. doi:10.1084/jem.20010938

Hamerman, J.A., K. Ogasawara, and L.L. Lanier. 2004. Cutting edge: Toll-like receptor signaling in macrophages induces ligands for the NKG2D receptor. *J. Immunol.* 172:2001–2005.

Honda, K., H. Yanai, H. Negishi, M. Asagiri, M. Sato, T. Mizutani, N. Shimada, Y. Ohba, A. Takaoka, N. Yoshida, and T. Taniguchi. 2005. IRF-7 is the master regulator of type-I interferon-dependent immune responses. *Nature.* 434:772–777. doi:10.1038/nature03464

Hornung, V., S. Rothenfusser, S. Britsch, A. Krug, B. Jahrsdörfer, T. Giese, S. Endres, and G. Hartmann. 2002. Quantitative expression of toll-like receptor 1-10 mRNA in cellular subsets of human peripheral blood mononuclear cells and sensitivity to CpG oligodeoxynucleotides. *J. Immunol.* 168:4531–4537.

Huntington, N.D., N. Legrand, N.L. Alves, B. Jaron, K. Weijer, A. Plet, E. Corcuff, E. Mortier, Y. Jacques, H. Spits, and J.P. Di Santo. 2009. IL-15 trans-presentation promotes human NK cell development and differentiation in vivo. *J. Exp. Med.* 206:25–34. doi:10.1084/jem.20082013

Iwasaki, A., and R. Medzhitov. 2004. Toll-like receptor control of the adaptive immune responses. *Nat. Immunol.* 5:987–995. doi:10.1038/ni1112

Kalinski, P., R.B. Mailliard, A. Giermasz, H.J. Zeh, P. Basse, D.L. Bartlett, J.M. Kirkwood, M.T. Lotze, and R.B. Herberman. 2005. Natural killer-dendritic cell cross-talk in cancer immunotherapy. *Expert Opin. Biol. Ther.* 5:1303–1315. doi:10.1517/14712598.5.10.1303

Kato, H., O. Takeuchi, S. Sato, M. Yoneyama, M. Yamamoto, K. Matsui, S. Uematsu, A. Jung, T. Kawai, K.J. Ishii, et al. 2006. Differential roles of MDA5 and RIG-I helicases in the recognition of RNA viruses. *Nature.* 441:101–105. doi:10.1038/nature04734

Kawai, T., K. Takahashi, S. Sato, C. Coban, H. Kumar, H. Kato, K.J. Ishii, O. Takeuchi, and S. Akira. 2005. IPS-1, an adaptor triggering RIG-I- and Mda5-mediated type I interferon induction. *Nat. Immunol.* 6:981–988. doi:10.1038/ni1243

Kubin, M.Z., D.L. Parshley, W. Din, J.Y. Waugh, T. Davis-Smith, C.A. Smith, B.M. Macduff, R.J. Armitage, W. Chin, L. Cassiano, et al. 1999. Molecular cloning and biological characterization of NK cell activation-inducing ligand, a counterstructure for CD48. *Eur. J. Immunol.* 29:3466–3477. doi:10.1002/(SICI)1521-4141(199911)29:11<3466::AID-IMMU3466>3.0.CO;2-9

Lee, A.E., L.A. Rogers, J.M. Longcroft, and R.E. Jeffery. 1990. Reduction of metastasis in a murine mammary tumour model by heparin and polyinosinic-polycytidylic acid. *Clin. Exp. Metastasis.* 8:165–171. doi:10.1007/BF00117789

Levy, S., and T. Shoham. 2005. The tetraspanin web modulates immune-signalling complexes. *Nat. Rev. Immunol.* 5:136–148. doi:10.1038/nri1548

Lucas, M., W. Schachterle, K. Oberle, P. Aichele, and A. Diefenbach. 2007. Dendritic cells prime natural killer cells by trans-presenting interleukin 15. *Immunity.* 26:503–517. doi:10.1016/j.immuni.2007.03.006

Masuda, H., Y. Saeki, M. Nomura, K. Shida, M. Matsumoto, M. Ui, L.L. Lanier, and T. Seya. 2002. High levels of RAE-1 isoforms on mouse tumor cell lines assessed by anti-"pan" RAE-1 antibody confer tumor susceptibility to NK cells. *Biochem. Biophys. Res. Commun.* 290:140–145. doi:10.1006/bbrc.2001.6165

Matsumoto, M., and T. Seya. 2008. TLR3: interferon induction by double-stranded RNA including poly(I:C). *Adv. Drug Deliv. Rev.* 60:805–812. doi:10.1016/j.addr.2007.11.005

McCartney, S., W. Vermi, S. Gilfillan, M. Cella, T.L. Murphy, R.D. Schreiber, K.M. Murphy, and M. Colonna. 2009. Distinct and complementary functions of MDA5 and TLR3 in poly(I:C)-mediated activation of mouse NK cells. *J. Exp. Med.* 206:2967–2976. doi:10.1084/jem.20091181

Medzhitov, R., and C.A. Janeway Jr. 1997. Innate immunity: the virtues of a nonclonal system of recognition. *Cell.* 91:295–298. doi:10.1016/S0092-8674(00)80412-2

Meylan, E., J. Curran, K. Hofmann, D. Moradpour, M. Binder, R. Bartenschlager, and J. Tschopp. 2005. Cardif is an adaptor protein in the RIG-I antiviral pathway and is targeted by hepatitis C virus. *Nature.* 437:1167–1172. doi:10.1038/nature04193

Miyake, T., Y. Kumagai, H. Kato, Z. Guo, K. Matsushita, T. Satoh, T. Kawagoe, H. Kumar, M.H. Jang, T. Kawai, et al. 2009. Poly I:C-induced activation of NK cells by CD8 alpha+ dendritic cells via the IPS-1 and TRIF-dependent pathways. *J. Immunol.* 183:2522–2528. doi:10.4049/jimmunol.0901500

Mukai, M., F. Imamura, M. Ayaki, K. Shinkai, T. Iwasaki, K. Murakami-Murofushi, H. Murofushi, S. Kobayashi, T. Yamamoto, H. Nakamura, and H. Akedo. 1999. Inhibition of tumor invasion and metastasis by a novel lysophosphatidic acid (cyclic LPA). *Int. J. Cancer.* 81:918–922. doi:10.1002/(SICI)1097-0215(19990611)81:6<918::AID-IJC13>3.0.CO;2-E

Newman, K.C., and E.M. Riley. 2007. Whatever turns you on: accessory-cell-dependent activation of NK cells by pathogens. *Nat. Rev. Immunol.* 7:279–291. doi:10.1038/nri2057

Nomura, M., Z. Zou, T. Joh, Y. Takihara, Y. Matsuda, and K. Shimada. 1996. Genomic structures and characterization of Rae1 family members encoding GPI-anchored cell surface proteins and expressed predominantly in embryonic mouse brain. *J. Biochem.* 120:987–995.

Ohteki, T., H. Tada, K. Ishida, T. Sato, C. Maki, T. Yamada, J. Hamuro, and S. Koyasu. 2006. Essential roles of DC-derived IL-15 as a mediator of inflammatory responses in vivo. *J. Exp. Med.* 203:2329–2338. doi:10.1084/jem.20061297

Oshiumi, H., M. Matsumoto, K. Funami, T. Akazawa, and T. Seya. 2003a. TICAM-1, an adaptor molecule that participates in Toll-like receptor 3-mediated interferon-beta induction. *Nat. Immunol.* 4:161–167. doi:10.1038/ni886

Oshiumi, H., M. Sasai, K. Shida, T. Fujita, M. Matsumoto, and T. Seya. 2003b. TIR-containing adapter molecule (TICAM)-2, a bridging adapter recruiting to toll-like receptor 4 TICAM-1 that induces interferon-beta. *J. Biol. Chem.* 278:49751–49762. doi:10.1074/jbc.M305820200

Sasai, M., M. Shingai, K. Funami, M. Yoneyama, T. Fujita, M. Matsumoto, and T. Seya. 2006. NAK-associated protein 1 participates in both the TLR3 and the cytoplasmic pathways in type I IFN induction. *J. Immunol.* 177:8676–8683.

Sato, M., H. Suemori, N. Hata, M. Asagiri, K. Ogasawara, K. Nakao, T. Nakaya, M. Katsuki, S. Noguchi, N. Tanaka, and T. Taniguchi. 2000. Distinct and essential roles of transcription factors IRF-3 and IRF-7 in response to viruses for IFN-alpha/beta gene induction. *Immunity.* 13:539–548. doi:10.1016/S1074-7613(00)00053-4

Seth, R.B., L. Sun, C.K. Ea, and Z.J. Chen. 2005. Identification and characterization of MAVS, a mitochondrial antiviral signaling protein that activates NF-kappaB and IRF 3. *Cell.* 122:669–682. doi:10.1016/j.cell.2005.08.012

Seya, T., and M. Matsumoto. 2009. The extrinsic RNA-sensing pathway for adjuvant immunotherapy of cancer. *Cancer Immunol. Immunother.* 58:1175–1184. doi:10.1007/s00262-008-0652-9

Sivori, S., M. Falco, M. Della Chiesa, S. Carlomagno, M. Vitale, L. Moretta, and A. Moretta. 2004. CpG and double-stranded RNA trigger human NK cells by Toll-like receptors: induction of cytokine release and cytotoxicity against tumors and dendritic cells. *Proc. Natl. Acad. Sci. USA.* 101:10116–10121. doi:10.1073/pnas.0403744101

Tanaka, H., Y. Mori, H. Ishii, and H. Akedo. 1988. Enhancement of metastatic capacity of fibroblast-tumor cell interaction in mice. *Cancer Res.* 48:1456–1459.

Tsuji, S., J. Uehori, M. Matsumoto, Y. Suzuki, A. Matsuhisa, K. Toyoshima, and T. Seya. 2001. Human intelectin is a novel soluble lectin that recognizes galactofuranose in carbohydrate chains of bacterial cell wall. *J. Biol. Chem.* 276:23456–23463. doi:10.1074/jbc.M103162200

Vivier, E., E. Tomasello, M. Baratin, T. Walzer, and S. Ugolini. 2008. Functions of natural killer cells. *Nat. Immunol.* 9:503–510. doi:10.1038/ni1582

Xu, L.G., Y.Y. Wang, K.J. Han, L.Y. Li, Z. Zhai, and H.B. Shu. 2005. VISA is an adapter protein required for virus-triggered IFN-beta signaling. *Mol. Cell.* 19:727–740. doi:10.1016/j.molcel.2005.08.014

Yamamoto, M., S. Sato, H. Hemmi, K. Hoshino, T. Kaisho, H. Sanjo, O. Takeuchi, M. Sugiyama, M. Okabe, K. Takeda, and S. Akira. 2003a. Role of adaptor TRIF in the MyD88-independent toll-like receptor signaling pathway. *Science.* 301:640–643. doi:10.1126/science.1087262

Yamamoto, M., S. Sato, H. Hemmi, S. Uematsu, K. Hoshino, T. Kaisho, O. Takeuchi, K. Takeda, and S. Akira. 2003b. TRAM is specifically involved in the Toll-like receptor 4-mediated MyD88-independent signaling pathway. *Nat. Immunol.* 4:1144–1150. doi:10.1038/ni986

Yoneyama, M., M. Kikuchi, T. Natsukawa, N. Shinobu, T. Imaizumi, M. Miyagishi, K. Taira, S. Akira, and T. Fujita. 2004. The RNA helicase RIG-I has an essential function in double-stranded RNA-induced innate antiviral responses. *Nat. Immunol.* 5:730–737. doi:10.1038/ni1087

Zanoni, I., M. Foti, P. Ricciardi-Castagnoli, and F. Granucci. 2005. TLR-dependent activation stimuli associated with Th1 responses confer NK cell stimulatory capacity to mouse dendritic cells. *J. Immunol.* 175:286–292.

Zou, Z., M. Nomura, Y. Takihara, T. Yasunaga, and K. Shimada. 1996. Isolation and characterization of retinoic acid-inducible cDNA clones in F9 cells: a novel cDNA family encodes cell surface proteins sharing partial homology with MHC class I molecules. *J. Biochem.* 119:319–328.

Y. Saitoh, MD
M. Ogawa, MD, PhD
Y. Naito, MD, PhD
Y. Komatsuzaki, MD
H. Tagaya, MD, PhD
K. Arima, MD, PhD
A. Tamaoka, MD, PhD
T. Kitamoto, MD, PhD
M. Murata, MD, PhD

DISCORDANT CLINICOPATHOLOGIC PHENOTYPES IN A JAPANESE KINDRED OF FATAL FAMILIAL INSOMNIA

The GAC→AAC mutation at codon 178 (D178N) of prion protein (PrP) gene (*PRNP*) results in 2 distinct clinicopathologic phenotypes dependent on codon 129 polymorphism of the mutant allele: fatal familial insomnia (FFI) with methionine encoded in codon 129 and familial Creutzfeldt-Jakob disease (CJD) with valine.[1,2] However, some D178N patients who had homozygosity for methionine at codon 129 (D178N-129MM) were reported recently to have the CJD phenotype.[3-5] The cause for these clinicopathologic diversities is unclear. We report a Japanese son–mother pair who presented with FFI and CJD phenotypes.

Case reports. ***Patient 1 (proband).*** A 54-year-old man, born to nonconsanguineous parents, developed dysphagia and loss of appetite. Later, he showed peculiar movement in sleep, followed by insomnia and hypersomnolence. Diplopia, intention tremor, ataxic gait, sleep apnea, fluctuant low-grade fever, tachycardia, hyperhidrosis, constipation, and impotence also

Figure **Histopathologic analysis and Western blot analysis**

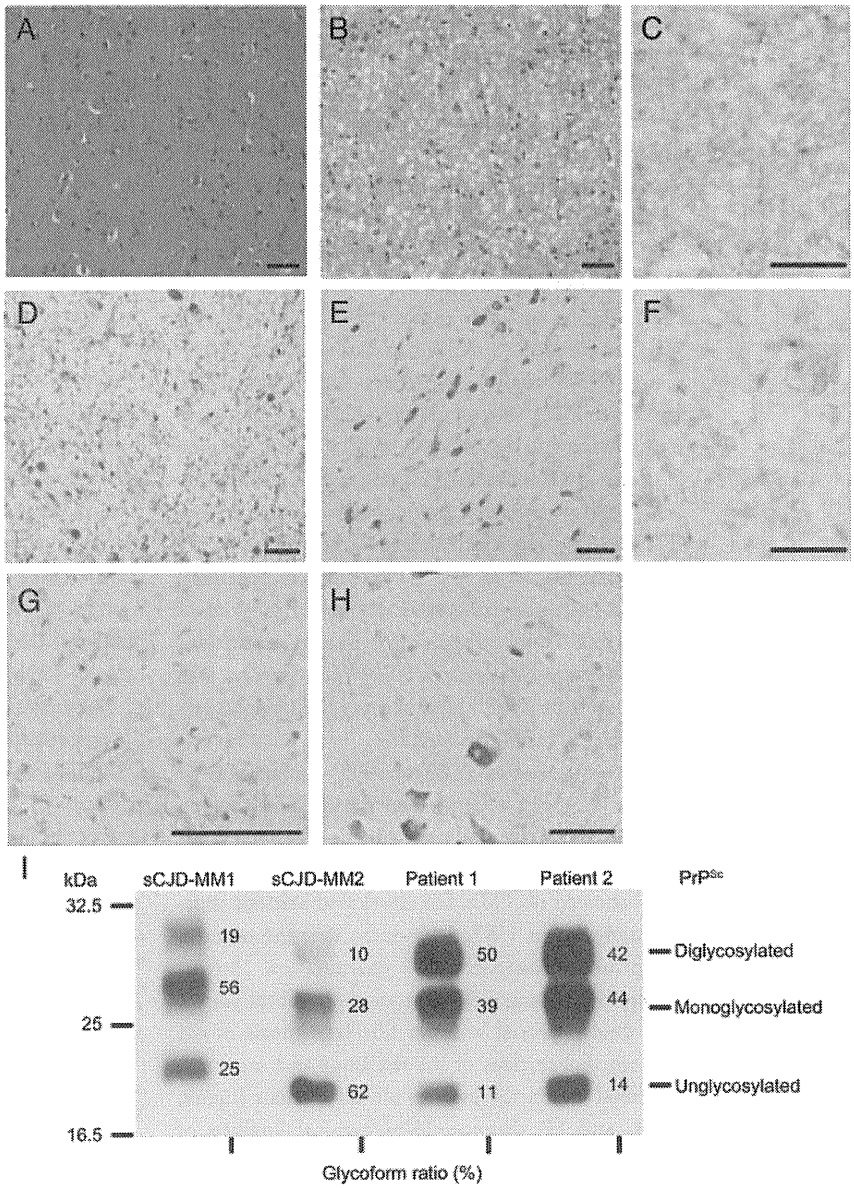

(A–H) Histopathologic findings of patient 1 (A, D, and G) and patient 2 (B, C, E, F, and H); hematoxylin and eosin staining of the frontal cortex (A and B), immunohistochemistry using anti-prion antibody (3F4; Signet Laboratories, Dedham, MA) of the frontal cortex (C) and thalamus (F), Klüver-Barrera staining of the thalamus (D and E) and inferior olivary nucleus (G and H). No spongiform changes were detected in the frontal cortex of patient 1 (or at best partial changes; not shown). In comparison, severe and fine spongiform changes and neuronal loss were detected in patient 2. Patient 1 showed severe neuronal loss and gliosis in the thalamus (D) and inferior olivary nucleus (G). In contrast, patient 2 showed neuronal loss and gliosis, which were mild in the thalamus (E) and moderate in the inferior olivary nucleus (H). Immunohistochemistry in patient 2 showed punctate and coarse granular deposits of pathologic prion protein (PrP^{Sc}) (C) and of the thalamus (F). There also was perivacuolar staining of PrP^{Sc} in places of the cerebral cortex. Coarse granular deposits of PrP^{Sc} in the thalamus were more prominent than that of the cerebral cortex in patient 2. However, immunohistochemistry did not show any PrP^{Sc} deposit throughout the brain in patient 1 (not shown). PrP^{Sc} plaques were not found in either patient. Bar = 50 μm (A, B, D, E, G, and H), 20 μm (C and F). (I) Western blot analysis of patient 1, patient 2, and 2 sporadic Creutzfeldt-Jakob disease (sCJD) patients as disease control was performed with 3F4. Samples of the left two lanes, sCJD-MM1 and sCJD-MM2, were extracted from the sCJD patients who were homozygous for methionine at codon 129 and the types of PrP^{Sc} were type 1 and type 2. The applied amount of frontal cortex tissue was 1.667 mg wet weight in patient 1 and 0.025 mg wet weight in patient 2. Note that both patients 1 and 2 had type 2 PrP^{Sc} as sCJD-MM2. The smallest fragment of PrP^{Sc}, which represents unglycosylated fragment, is weaker than the other 2 fragments in both patients. The PrP^{Sc} glycoform ratio, quantified with Quantity One software using an imaging device, Vasa Doc 5000 (BioRad Laboratories), clarifies that the glycosylation pattern of patient 1 and patient 2 is different from that of sCJD-MM1 and sCJD-MM2. Note the strong band of PrP^{Sc} in patient 2 although a smaller amount of brain tissue was applied than that of patient 1.

followed. He was admitted to hospital 7 months after the onset of symptoms.

Neurologic examination showed mild memory disturbance, cerebellar ataxia, myoclonus, brisk deep tendon reflexes, sleep apnea, and dysautonomia. He did not show akinetic mutism. He moved continuously during sleep. EEG showed no periodic synchronous discharge (PSD), and polysomnography showed loss of deep sleep and marked reduction of REM sleep. Brain MRI showed only mild atrophy. In the cerebral cortex and thalamus, hypoperfusion and hypometabolism were detected by SPECT with ^{99m}Tc-ECD and PET with ^{18}F-2-fluorodeoxy-D-glucose. He died 13 months after the onset of symptoms. *PRNP* analysis, with informed consent, on leukocyte DNA showed D178N-129MM. Histologic examination showed spongiform changes limited to the cingulate gyrus and subiculum, and severe neuronal loss and fibrillary gliosis in the centromedian and dorsomedial nucleus of the thalamus and in the inferior olivary nucleus (figure, A, D, and G). Immunohistochemical analysis showed no pathologic PrP (PrP^{Sc}) deposition in the cerebral cortex, thalamus, or inferior olivary nucleus. Western blot analysis (WB) showed very small amount of type 2 PrP^{Sc} and the same glycosylation pattern of PrP^{Sc} as FFI (figure, I).[6,7]

Patient 2 (mother). A 60-year-old woman showed rapidly progressive dementia. She became mute 5 months later. Neurologic examination showed rigidity and brisk deep tendon reflexes, but no ataxia. EEG showed no PSD. She developed akinetic mutism and died in 1987, 14 months after the onset of symptoms. Histopathologic examination showed spongiform changes throughout the cerebral cortex, and mild neuronal loss and fibrillary gliosis in the dorsomedial nucleus of the thalamus and moderate neuronal loss in the inferior olivary nucleus (figure, B, E, and H). Immunohistochemical analysis of PrP^{Sc} visualized punctate and coarse granular deposits throughout the cerebral cortex (figure, C), and coarse granular deposits in thalamus (figure, F). Although the clinical course and histopathologic findings of patient 2 were compatible with CJD phenotype, the type and glycosylation pattern, including glycoform ratio, of PrP^{Sc} analyzed by WB were the same as patient 1, who presented as typical FFI (figure, I). However, a larger amount of PrP^{Sc} was detected than that of patient 1. *PRNP* analysis on preserved frozen brain tissue, performed with informed consent, revealed exactly the same as patient 1, D178N-129MM.

Discussion. A few reports describe the CJD phenotype in a genetically confirmed D178N-129MM kindred,[3-5] although one kindred showed both FFI and CJD phenotypes within the same family.[5] That kindred and ours indicate that certain factors other than codon 129 polymorphism in the normal allele determine the clinicopathologic phenotype of D178N-129MM.

Our WB suggests the causes of this clinicopathologic diversity. The detection of the larger amount of PrP^{Sc} in patient 2 than in patient 1 may indicate that the amount of PrP^{Sc} is related to the clinicopathologic D178N-129MM phenotype. However, the mechanism by which there is an increased amount of PrP^{Sc} in this kindred is unknown. In addition, that both patients have the same type 2 PrP^{Sc} indicates that the type of PrP^{Sc} may not be related to the D178N-129MM phenotype, unlike sporadic CJD.[6] Finally, the result that the both patients have the same glycosylation pattern of PrP^{Sc}, including glycoform ratio, also indicates that the D178N-129MM phenotype may not be influenced by glycosylation pattern. However, because the glycosylation pattern reflects both the degree of glycosylation and location at which the PrP is cleaved by protease, careful investigation of the glycosylation of PrP is necessary to interpret the clinicopathologic diversity of this D178N-129MM kindred.

The majority of D178N-129 M kindred follows the genetic pattern[1,2]; however, there are a few D178N-129MM kindred who presented with both FFI and CJD phenotypes. Therefore, our kindred may be an exception, suggesting the importance of WB to investigate this rare syndrome.

From the Departments of Neurology (Y.S., M.O., M.M.), Laboratory Medicine (H.T., K.A.), and Psychiatry (K.A.), National Center Hospital of Neurology and Psychiatry, Tokyo; Department of Degenerative Neurological Diseases (Y.S.), National Institute of Neuroscience, National Center of Neurology and Psychiatry, Tokyo; Hatsuishi Hospital (Y.N., Y.K.), Chiba; Department of Neurology (Y.N.), Mie University Graduate School of Medicine, Mie; Miraidaira Clinic (Y.K.), Ibaraki; Mental Health Department of Health Science (H.T.), School of Allied Health Sciences, Kitasato University, Kanagawa; Department of Neurology (A.T.), Doctoral Program in Medical Sciences for Control of Pathological Processes, Graduate School of Comprehensive Human Sciences, University of Tsukuba, Ibaraki; and Division of CJD Science and Technology (T.K.), Department of Prion Research, Tohoku University Graduate School of Medicine, Miyagi, Japan.

Study funding: Supported by a grant from the Research Committee on Prion Diseases and Slow Virus Infection and Research Grant 19A-4 for Nervous and Mental Disorders, Ministry of Health, Labour, and Welfare, Japan.

Disclosure: Dr. Saitoh and Dr. Ogawa report no disclosures. Dr. Naito has received research support from Asubio Pharmaceuticals, Inc., Janssen, Otsuka Pharmaceutical Co. Ltd., and Ono Pharmaceutical Co. Ltd. Dr. Komatsuzaki reports no disclosures. Dr. Tagaya received funding for travel from Sanofi-Aventis, serves on speakers' bureaus for Sanofi-Aventis, Astellas Pharma Inc., Takeda Pharmaceutical Company Limited, Boehringer Ingelheim, and KYORIN Pharmaceutical Co., Ltd., and receives research support from the Ministry of Health, Labour, and Welfare, Japan, Ministry of Education, Culture, Science and Technology, Japan, and Kitasato University School of Allied Health Sciences. Dr. Arima reports no disclosures. Dr. Tamaoka serves on a scientific advisory board for

Chugai Pharmaceutical Company and has received research support from Sankyo Seimei, Ministry of Health, Labour, and Welfare, Japan, and Ministry of Education, Culture, Science and Technology, Japan. Dr. Kitamoto reports no disclosures. Dr. Murata serves on speakers' bureaus for Dainippon Sumitomo Pharma Co., Ltd., Novartis, Boehringer Ingelheim, and GlaxoSmithKline and receives research support from the Ministry of Health, Labour, and Welfare, Japan.

Received February 1, 2009. Accepted in final form October 13, 2009.

Address correspondence and reprint requests to Dr. Miho Murata, Department of Neurology, National Center Hospital of Neurology and Psychiatry, 4-1-1 Ogawahigashimachi, Kodaira, Tokyo 187-8551, Japan; mihom@ncnp.go.jp

ACKNOWLEDGMENT

The authors thank Dr. Hidehiro Mizusawa, Department of Neurology and Neurological Science, Graduate School, Tokyo Medical and Dental University; Dr. Akihide Mochizuki, Department of Neurology, Doctoral Program in Medical Sciences for Control of Pathologic Processes, Graduate School of Comprehensive Human Sciences, University of Tsukuba; and Dr. Yuko Saito, Department of Laboratory Medicine, National Center Hospital of Neurology and Psychiatry, for their comments on the histopathologic data.

1. Medori R, Tritschler HJ, LeBlanc A, et al. Fatal familial insomnia, a prion disease with a mutation at codon 178 of the prion protein gene. N Engl J Med 1992;326:444–449.
2. Goldfarb LG, Petersen RB, Tabaton M, et al. Fatal familial insomnia and familial Creutzfeldt-Jakob disease: disease phenotype determined by a DNA polymorphism. Science 1992;258:806–808.
3. McLean CA, Storey E, Gardner RJ, Tannenberg AE, Cervenakova L, Brown P. The D178N (cis-129M) "fatal familial insomnia" mutation associated with diverse clinicopathologic phenotypes in an Australian kindred. Neurology 1997;49:552–558.
4. Harder A, Jendroska K, Kreuz F, et al. Novel twelve-generation kindred of fatal familial insomnia from Germany representing the entire spectrum of disease expression. Am J Med Genet 1999;87:311–316.
5. Zarranz JJ, Digon A, Atares B, et al. Phenotypic variability in familial prion diseases due to the D178N mutation. J Neurol Neurosurg Psychiatry 2005;76:1491–1496.
6. Parchi P, Giese A, Capellari S, et al. Classification of sporadic Creutzfeldt-Jakob disease based on molecular and phenotypic analysis of 300 subjects. Ann Neurol 1999;46:224–233.
7. Monari L, Chen SG, Brown P, et al. Fatal familial insomnia and familial Creutzfeldt-Jakob disease: different prion proteins determined by a DNA polymorphism. Proc Natl Acad Sci USA 1994;91:2839–2842.

Cell Mol Neurobiol (2010) 30:415–426
DOI 10.1007/s10571-009-9466-3

ORIGINAL RESEARCH

Stable Expression of Neurogenin 1 Induces LGR5, a Novel Stem Cell Marker, in an Immortalized Human Neural Stem Cell Line HB1.F3

Jun-ichi Satoh · Shinya Obayashi · Hiroko Tabunoki · Taeko Wakana · Seung U. Kim

Received: 15 August 2009 / Accepted: 25 September 2009 / Published online: 8 October 2009

Abstract Neural stem cells (NSC) with self-renewal and multipotent properties serve as an ideal cell source for transplantation to treat spinal cord injury, stroke, and neurodegenerative diseases. To efficiently induce neuronal lineage cells from NSC for neuron replacement therapy, we should clarify the intrinsic genetic programs involved in a time- and place-specific regulation of human NSC differentiation. Recently, we established an immortalized human NSC clone HB1.F3 to provide an unlimited NSC source applicable to genetic manipulation for cell-based therapy. To investigate a role of neurogenin 1 (Ngn1), a proneural basic helix-loop-helix (bHLH) transcription factor, in human NSC differentiation, we established a clone derived from F3 stably overexpressing Ngn1. Genome-wide gene expression profiling identified 250 upregulated genes and 338 downregulated genes in Ngn1-overexpressing F3 cells (F3-Ngn1) versus wild-type F3 cells (F3-WT). Notably, leucine-rich repeat-containing G protein-coupled receptor 5 (LGR5), a novel stem cell marker, showed an 167-fold increase in F3-Ngn1, although transient overexpression of Ngn1 did not induce upregulation of LGR5, suggesting that LGR5 is not a direct transcriptional target of Ngn1. KeyMolnet, a bioinformatics tool for analyzing molecular relations on a comprehensive knowledgebase, suggests that the molecular network of differentially expressed genes involves the complex interaction of networks regulated by multiple transcription factors. Gene ontology (GO) terms of development and morphogenesis are enriched in upregulated genes, while those of extracellular matrix and adhesion are enriched in downregulated genes. These results suggest that stable expression of a single gene Ngn1 in F3 cells induces not simply neurogenic but multifunctional changes that potentially affect the differentiation of human NSC via a reorganization of complex gene regulatory networks.

Keywords HB1.F3 · KeyMolnet · LGR5 · Microarray · Neural stem cells · Neurogenin 1

Abbreviations

bHLH	Basic helix-loop-helix
CNS	Central nervous system
DAVID	Database for annotation visualization and integrated discovery
DEG	Differentially expressed genes
FBS	Fetal bovine serum
GAS2	Growth arrest-specific 2
GO	Gene ontology
HAS2	Hyaluronan synthase 2
LGR5	Leucine-rich repeat-containing G protein-coupled receptor 5
MMP9	Matrix metallopeptidase 9
Ngn1	Neurogenin 1

Electronic supplementary material The online version of this article (doi:10.1007/s10571-009-9466-3) contains supplementary material, which is available to authorized users.

J. Satoh (✉) · S. Obayashi · H. Tabunoki · T. Wakana
Department of Bioinformatics and Molecular Neuropathology, Meiji Pharmaceutical University, 2-522-1 Noshio, Kiyose, Tokyo 204-8588, Japan
e-mail: satoj@my-pharm.ac.jp

S. U. Kim
Division of Neurology, Department of Medicine, University of British Columbia Hospital, University of British Columbia, Vancouver, BC, Canada

S. U. Kim
Medical Research Institute, Chung-Ang University College of Medicine, Seoul, Korea

NPC	Neural progenitor cells
NSC	Neural stem cells
ORF	Open-reading frame
RMA	Robust multiarray average
RT-PCR	Reverse transcription-polymerase chain reaction
SHH	Sonic hedgehog homolog
Wnt	Wingless-type MMTV integration site family

Introduction

Neural stem cells (NSC) with self-renewal and multipotent properties serve as an ideal cell source for transplantation to treat spinal cord injury, stroke, and neurodegenerative diseases (Kim 2004; Kim and de Vellis 2009). To efficiently induce neuronal lineage cells from NSC for neuron replacement therapy, we should clarify the intrinsic genetic programs involved in a time- and place-specific regulation of human NSC differentiation. Previously, we found that primary cultures of human neural progenitor cells (NPC) exhibit an intrinsic capacity to differentiate into astrocytes in response to bone morphogenic protein 4 (BMP4) included in the serum (Obayashi et al. 2009). This might be a major hindrance against the proper commitment to neuronal linage cells following transplantation of NSC in vivo. Recently, we established an immortalized human NSC clone HB1.F3 by retroviral vector-mediated v-myc gene transfer into fetal human telencephalon cell cultures (Kim 2004). HB1.F3 cells could provide an unlimited NSC source applicable to genetic manipulation ex vivo for cell-based therapy. Actually, F3 cells stably expressing therapeutic genes migrate and integrate into target brain tissues upon transplantation in animal models of Parkinson disease, Huntington disease, and amyotrophic lateral sclerosis, and they differentiate into neurons, followed by an enhanced functional recovery (Kim et al. 2006; Kim and de Vellis 2009).

Neurogenin-1 (NEUROG1, Ngn1) is a member of proneural basic helix-loop-helix (bHLH) transcription factors that promote neurogenesis by activating a battery of target genes, including the NeuroD family of bHLH transcription factors (Morrison 2001). During embryogenesis, Ngn1 is expressed in NPC distributed in dorsal root ganglia (DRG), dorsal and ventral regions of the neural tube, dorsal telencephalon, and specific regions within the midbrain and hindbrain (Sommer et al. 1996). Although there exists a functional redundancy among Ngn1, Ngn2, and Ngn3, Ngn1-deficient mice failed to generate a $TrkA^+$ subset of cervical DRG neurons (Ma et al. 1999). Overexpression of Ngn1 induces neurite outgrowth in F11 rat DRG and mouse neuroblastoma hybrid cells (Kim et al. 2002). Stable expression of Ngn1 induces neuronal differentiation of pluripotent mouse embryonal carcinoma P19 cells (Kim et al. 2004). Ngn1 inhibits differentiation of rat NSC into astrocytes by sequestering a transcriptional coactivator complex composed of CBP and SMAD1 and blocking activation of STAT transcription factors (Sun et al. 2001).

In the present study, to investigate the role of Ngn1 in human NSC differentiation, we established a clonal cell line stably overexpressing Ngn1 by retroviral vector-mediated gene transfer into HB1.F3 cells. Then, we studied genome-wide gene expression profiles of Ngn1-overexpressing F3 cells (F3-Ngn1) and wild-type F3 cells (F3-WT) by using whole genome DNA microarrays. As a result, we unexpectedly found that stable expression of a single gene Ngn1 in F3 cells induced a robust upregulation of leucine-rich repeat-containing G protein-coupled receptor 5 (LGR5), a recently identified marker for intestine and hair follicle stem cells (Barker et al. 2007; Jaks et al. 2008; Sato et al. 2009). Our results suggested that stable expression of Ngn1 in human NSC cells induces not only simply neurogenic but also multifunctional changes that potentially affect the differentiation of NSC via a reorganization of complex gene regulatory networks.

Methods

Human Neural Stem Cell Clone HB1.F3 and Its Derivative HB1.F3-Ngn1

Primary cultures of fetal human telencephalon cells were transformed with a retroviral vector pLSNmyc carrying the v-myc oncogene and the neomycin resistance gene. Following selection with G418, a single continuously dividing clone with a capacity to self-renew and differentiate into neurons and glial cells both in vitro and in vivo was isolated and designated HB1.F3 (Kim 2004). It carried normal human karyotype of 46 XX. After transducing a retroviral vector pBabePNgn1 carrying the open-reading frame (ORF) of the human Ngn1 gene and the puromycin resistance gene into HB1.F3 cells, a single puromycin-resistant clone was selected, expanded, and designated HB1.F3-Ngn1. In the present study, the wild-type HB1.F3 cells and the HB1.F3-Ngn1 cells are abbreviated as F3-WT and F3-Ngn1. They were incubated in the feeding medium composed of Dulbecco's modified Eagle's medium (DMEM) (Invitrogen, Carlsbad, CA, USA) supplemented with 10% fetal bovine serum (FBS), 100 U/ml penicillin and 100 μg/ml streptomycin. The medium was renewed every 3 days.

Microarray Analysis

Total RNA was isolated from subconfluent cells by using the TRIZOL Plus RNA Purification kit (Invitrogen). The

quality of total RNA was evaluated on Agilent 2100 Bioanalyzer (Agilent Technologies, Palo Alto, CA, USA). One hundred nanograms of total RNA was processed for cRNA synthesis, fragmentation, and terminal labeling with the GeneChip Whole Transcript Sense Target Labeling and Control Reagents (Affymetrix, Santa Clara, CA, USA). Then, it was processed for hybridization at 45°C for 17 h with Human Gene 1.0 ST Array (Affymetrix) containing 28,869 genes with approximately 26 probes per each gene that spread across the full length of the gene. The arrays were washed in the GeneChip Fluidic Station 450 (Affymetrix), and scanned by the GeneChip Scanner 3000 7G (Affymetrix). The data expressed as CEL files were normalized by the robust multiarray average (RMA) method with the Expression Console software version 1.1 (Affymetrix). By comparing the signal intensity levels between F3-WT and F3-Ngn1, the genes exhibiting either greater than twofold upregulation or smaller than 0.5-fold downregulation are considered as differentially expressed genes (DEG). To perform unsupervised clustering analysis of gene expression profiles, the CEL file-based data were imported to GeneSpring GX10 (Agilent).

Molecular Network Analysis

KeyMolnet is a comprehensive knowledgebase, originally established by the Institute of Medicinal Molecular Design (IMMD), Tokyo, Japan (Sato et al. 2005). It contains numerous contents of human genes, molecules and molecular relations, diseases, pathways, and drugs, all of which are manually collected, carefully curated, and regularly updated by expert biologists. The database is categorized into the core contents collected from selected review articles with the highest reliability or the secondary contents extracted from abstracts of PubMed database and Human Protein Reference database (HPRD). By importing the list of Entrez Gene ID and signal intensity data, KeyMolnet automatically provides corresponding molecules as a node on networks. Among various network-searching algorithms, the "N-points to N-points" search extracts the molecular network with the shortest route connecting the starting point molecules and the end point molecules. The generated network was compared side by side with 403 human canonical pathways of the KeyMolnet library. The algorithm counting the number of overlapping molecular relations between the extracted network and the canonical pathway makes it possible to identify the canonical pathway showing the most significant contribution to the extracted network. The significance in the similarity between both is scored following the formula, where O = the number of overlapping molecular relations between the extracted network and the canonical pathway, V = the number of molecular relations located in the extracted network, C = the number of molecular relations located in the canonical pathway, T = the number of total molecular relations composed of approximately 110,000 sets, and the X = the sigma variable that defines coincidence.

$$\text{Score} = -\log_2(\text{Score (p)}) \quad \text{Score(p)} = \sum_{x=O}^{\text{Min}(C,V)} f(x)$$

$$f(x) = {}_C C_x \cdot {}_{T-C} C_{V-x} / {}_T C_V$$

Gene Annotation Analysis

Functional annotation of differentially expressed genes was searched by the web-accessible program named Database for Annotation, Visualization, and Integrated Discovery (DAVID) version 2008, National Institute of Allergy and Infectious Diseases (NIAID), NIH (david.abcc.ncifcrf.gov) (Huang da et al. 2009). It covers more than 40 annotation categories, including Gene ontology (GO) terms, protein–protein interactions, protein functional domains, disease associations, biological pathways, sequence general features, homologies, gene functional summaries, and tissue expressions. By importing the list of Entrez Gene ID, this program creates the functional annotation chart, an annotation-term-focused view that lists annotation terms and their associated genes under study. To avoid excessive counting of duplicated genes, the Fisher Exact statistics is calculated based on corresponding DAVID gene IDs by which all redundancies in original IDs are removed.

Real-Time RT-PCR Analysis

DNase-treated total cellular RNA was processed for cDNA synthesis using oligo(dT)$_{12-18}$ primers and SuperScript II reverse transcriptase (Invitrogen). Then, cDNA was amplified by PCR in LightCycler ST300 (Roche Diagnostics, Tokyo, Japan) using SYBR Green I and primer sets listed in Table 1. The expression levels of target genes were standardized against those of the glyceraldehyde-3-phosphate dehydrogenase (G3PDH) gene detected in parallel in identical cDNA samples. All the assays were performed in triplicate.

In some experiments, the ORF of Ngn1 was amplified by PCR using PfuTurbo DNA polymerase (Stratagene, La Jolla, CA, USA) and primer sets listed in Table 1. It was then cloned into the mammalian expression vector p3XFLAG-CMV7.1 (Sigma, St. Louis, MO, USA) to express a fusion protein with an N-terminal Flag tag. At 48 h after transfection of the vector in F3-WT cells by Lipofectamine 2000 reagent (Invitrogen), the cells were processed for real-time RT-PCR analysis of LGR5 and Western blot analysis of a Flag-fusion protein with anti-Flag M2 antibody (Sigma).

Table 1 Primers for RT-PCR and cloning utilized in the present study

Genes	GenBank accession no.	Sense primers	Antisense primers
NES	NM_006617	5′ctgctcaggagcagcactcttaac3′	5′cttagcctatgagatggagcaggc3′
LGR5	NM_003667	5′aacagtcctgtgactcaactcaag3′	5′ttagagacatgggacaaatgccac3′
GAS2	NM_005256	5′acaaacatgtcatggtccgtgtgg3′	5′aactggcagagaccaccaagtagt3′
HAS2	NM_005328	5′gccagctgccttagaggaaatatc3′	5′atggttttccttcctgatgtgccc3′
MMP9	NM_004994	5′tcttccagtaccgagagaaagcct3′	5′ctgcaggatgtcataggtcacgta3′
NEUROG1	NM_006161	5′ttcctcaccgacgaggaagactgt3′	5′tcaagttgtgcatgcggttgcgct3′
NEUROG1 for cloning	NM_006161	5′cggaattccccagcccgccttgagacctgc3′	5′cgggatcccgctagtggtaaggaatgaaac3′
G3PDH	NM_002046	5′ccatgttcgtcatgggtgtgaacca3′	5′gccagtagaggcagggatgatgttc3′

NES Nestin, *LGR5* leucine-rich repeat-containing G protein-coupled receptor 5, *GAS2* growth arrest-specific 2, *HAS2* hyaluronan synthase 2, *MMP9* matrix metallopeptidase 9, *NEUROG1* neurogenin 1, and *G3PDH* glyceraldehyde-3-phosphate dehydrogenase

Western Blot Analysis

To prepare total protein extract, the cells were homogenized in RIPA buffer containing a cocktail of protease inhibitors (Sigma). After separation on a 12% SDS-PAGE gel, the protein was transferred onto a nitrocellulose membrane, and the blot was incubated with rabbit polyclonal anti-LGR5 antibody (AP2745d) (ABGENT, Flanders Court, San Diego, CA, USA). Then, it was labeled with HRP-conjugated anti-rabbit IgG (Santa Cruz Biotechnology, Santa Cruz, CA, USA). The specific reaction was visualized by exposing of the blot to a chemiluminescence substrate (Pierce, Rockford, IL, USA). After the antibodies were stripped by incubating the membrane at 50°C for 30 min in stripping buffer, composed of 62.5 mM Tris–HCl, pH 6.7, 2% SDS, and 100 mM 2-mercaptoethanol, it was processed for relabeling with anti-Hsp60 antibody (N-20; Santa Cruz Biotechnology), an internal control for protein loading.

Results

Overexpression of Neurogenin 1 in F3-Ngn1 Cells

When incubated in the feeding medium, both F3-WT and F3-Ngn1 cells proliferated continuously with a doubling time ranging from 3 to 7 days. Although they were morphologically different, i.e. F3-WT exhibited a fusiform morphology, while F3-Ngn1 exhibited a cuboidal appearance (Fig. 1A, panels a and b), both of them expressed nestin but did not form a neurosphere when cultured in the feeding medium. The levels of expression of nestin mRNA were higher in F3-Ngn1 than F3-WT (Fig. 1B, panel a, lanes 1 and 2). Importantly, only F3-Ngn1 expressed Ngn1 mRNA (Fig. 1B, panel b, lanes 1 and 2).

We conducted genome-wide gene expression profiling of F3-WT and F3-Ngn1 by using two sets of Human Gene 1.0 ST Array for each, followed by two comparisons composed of F3-WT array-1 (WT-1) versus F3-Ngn1 array-1 (NGN-1) and F3-WT array-2 (WT-2) versus F3-Ngn1 array-2 (NGN-2). Unsupervised clustering analysis of these data clearly separated the cluster of F3-Ngn1 from that of F3-WT, based on gene expression profiles of 59 genes differentially expressed between both cell types (Fig. 2). The gene expression profile of WT-1 was similar to that of WT-2, while the gene expression profiles of NGN-1 and NGN-2 were almost identical, supporting the reproducibility among the results of repeated microarray analysis (Fig. 2). The analysis of individual probe data identified significant upregulation of Ngn1 ORF expression

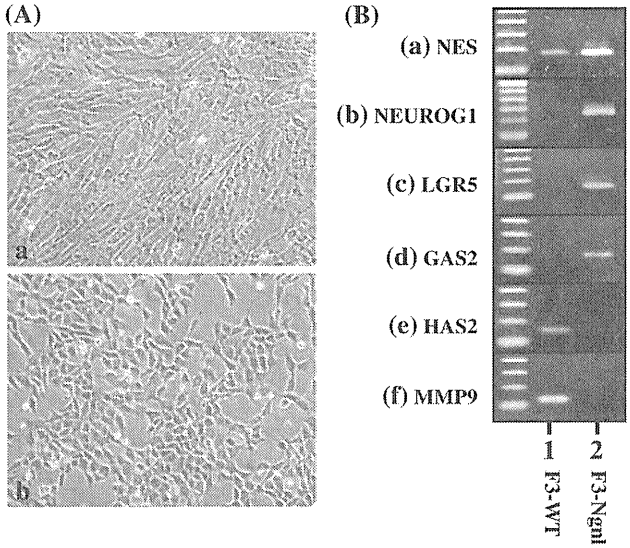

Fig. 1 Characterization of phenotypes of F3-WT and F3-Ngn1 cells. A Phase contrast photomicrograph. Both F3-WT cells (panel *a*) and F3-Ngn1 cells (panel *b*) were incubated in the feeding medium at a subconfluent density. B RT-PCR analysis. cDNA prepared from F3-WT cells (lane 1) and F3-Ngn1 cells (lane 2) was amplified by PCR for 30 cycles using primer sets listed in Table 1. The panels (*a–f*) represent (*a*) nestin (NES), (*b*) neurogenin 1 (NEUROG1), (*c*) leucine-rich repeat-containing G protein-coupled receptor 5 (LGR5), (*d*) growth arrest-specific 2 (GAS2), (*e*) hyaluronan synthase 2 (HAS2), and (*f*) matrix metallopeptidase 9 (MMP9)

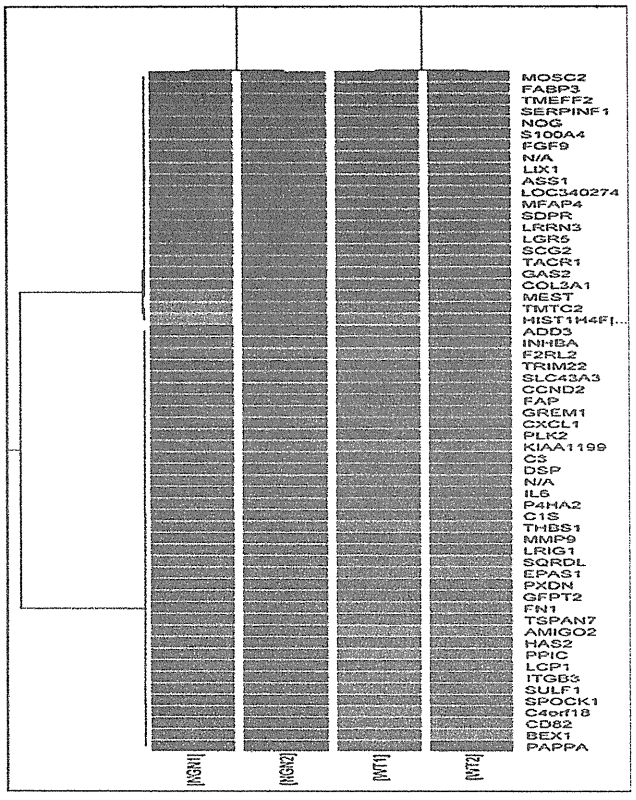

Fig. 2 Clustering analysis of gene expression profiles of F3-WT and F3-Ngn1 cells. Genome-wide gene expression profiling of F3-WT and F3-Ngn1 was performed by using two sets of Human Gene 1.0 ST Array for each, followed by two comparisons composed of WT array-1 (WT1) versus Ngn1 array-1 (NGN1) and WT array-2 (WT2) versus Ngn1 array-2 (NGN2). The microarray data are processed for unsupervised clustering analysis on GeneSpring GX10. A set of 59 differentially expressed genes between both cell types separated the cluster of F3-Ngn1 from that of F3-WT. The heat map represents upregulated genes (*orange*) and downregulated genes (*blue*)

in F3-Ngn1 cells (Supplementary Fig. 1). However, the Affymetrix GeneChip Command Console (AGCC) algorithm that calculates the cumulative gene expression levels excluded Ngn1 from the group of upregulated genes in F3-Ngn1 owing to low baseline expression of Ngn1 in the set of probes distributed outside its ORF on Human Gene 1.0 ST Array.

Microarray Analysis Identifies a Robust Induction of LGR5 in F3-Ngn1 Cells

Microarray analysis identified total 588 differentially expressed genes (DEG), composed of 250 upregulated genes and 338 downregulated genes in F3-Ngn1 versus F3-WT (see Supplementary Tables 1 and 2 for the complete lists). Top 20 upregulated genes are shown in Table 2. Notably, LGR5, a novel stem cell marker (Barker et al. 2007; Jaks et al. 2008; Sato et al. 2009), showed an 167-fold increase in F3-Ngn1 (Table 2; Fig. 3).

In view of cell type-specific markers for NSC, neurons, and glial cells, nestin (NES) exhibited a 3.1-fold increase in F3-Ngn1 (Supplementary Table 1; Fig. 3), consistent with RT-PCR results (Fig. 1B, panel a, lanes 1 and 2). However, the expression of other NSC-specific markers, such as musashi homolog 1 (MSI1) and ATP-binding cassette sub-family G member 2 (ABCG2), was not elevated in F3-Ngn1 (Fig. 3). Although neurofilament medium polypeptide (NEFM) showed a 2.1-fold increase, the expression of other neuron-specific markers, such as neurofilament heavy polypeptide (NEFH), enolase 2 (ENO2), and tubulin beta 3 (TUBB3), was not substantially upregulated in F3-Ngn1 (Fig. 3). The expression of astroglial (GFAP), oligodendroglial (MBP, MOG, and CNP), and microglial (CD68) markers remained unaltered (Fig. 3). Furthermore, NEUROD1, a putative Ngn-1 target gene,[5,10] was not upregulated in F3-Ngn1 (Fig. 3).

Top 20 downregulated genes are shown in Table 3. It is worthy to note that the great majority of top 20 downregulated genes are categorized as extracellular matrix-associated proteins.

RT-PCR and Western Blot Analysis Validated the Results of Microarray Analysis

Both the conventional RT-PCR and real-time RT-PCR analysis validated marked upregulation of LGR5 and GAS2, and remarkable downregulation of HAS2 and MMP9 in F3-Ngn1 (Fig. 1B, panels c–f, lanes 1 and 2; Fig. 4, panels a–d). Western blot analysis verified LGR5 protein expression exclusively in F3-Ngn1 (Fig. 4, panel e, lane 2).

To address the question whether LGR5 is a direct target for Ngn1, an expression vector of either Ngn1 or green fluorescent protein (GFP) was transfected in F3-WT cells (Fig. 5a, upper panel, lanes 1 and 2). At 48 h after transfection, the cells were processed for real-time RT-PCR analysis. Transient overexpression of Ngn1 did not induce LGR5 expression in F3-WT, suggesting that LGR5 is not a direct transcriptional target of Ngn1 (Fig. 5b).

An Involvement of the Complex Interaction of Networks Regulated by Multiple Transcription Factors in Development of F3-Ngn1 Cells

To clarify the molecular network of the genes differentially expressed between F3-WT and F3-Ngn1, we imported microarray data into KeyMolnet, a bioinformatics tool for analyzing molecular relations on a comprehensive knowledgebase. When Entrez Gene ID and expression levels of 588 DEG were imported, KeyMolnet recognized a set of 51 non-annotated genes to be removed. Then, it extracted 787

Table 2 Top 20 upregulated genes in F3 cells following stable expression of neurogenin 1

No.	Gene symbol	Fold change	Entrez gene ID	Gene name	Putative function
1	LGR5	166.623	8549	Leucine-rich repeat-containing G protein-coupled receptor 5	An orphan G protein-coupled receptor of the glycoprotein hormone receptor subfamily
2	GAS2	32.861	2620	Growth arrest-specific 2	A caspase-3 substrate that plays a role in regulating cell shape changes during apoptosis
3	FABP3	32.739	2170	Fatty acid-binding protein 3, muscle and heart (mammary-derived growth inhibitor)	A protein involved in intracellular metabolism of long-chain fatty acids and modulation of cell growth and proliferation
4	TMEFF2	28.233	23671	Transmembrane protein with EGF-like and two follistatin-like domains 2	A secreted protein with a EGF-like domain that promotes survival of hippocampal and mesencephalic neurons
5	LRRN3	24.284	54674	Leucine-rich repeat neuronal 3	An integral membrane protein of unknown function
6	SCG2	13.841	7857	Secretogranin II (chromogranin C)	A secretory protein involved in regulation of neurogenesis and angiogenesis
7	MFAP4	13.429	4239	Microfibrillar-associated protein 4	An extracellular matrix protein binding to both collagen and carbohydrate involved in cell adhesion
8	HIST1H4F	11.875	8361	H4 histone, family 2	A member of the histone H4 family that constitutes the nucleosome structure
9	TACR1	11.35	6869	Tachykinin receptor 1	A neurokinin receptor selective for substance P
10	COL3A1	10.828	1281	Collagen, type III, alpha 1	The pro-alpha 1 chains of type III collagen that constitutes a major component of the extracellular matrix
11	SDPR	9.975	8436	Serum deprivation response (phosphatidylserine-binding protein)	A calcium-independent phospholipid-binding protein that serves as a substrate of protein kinase C
12	TMTC2	9.744	160335	Transmembrane and tetratricopeptide repeat containing 2	An integral membrane protein of unknown function
13	FGF9	9.38	2254	Fibroblast growth factor 9 (glia-activating factor)	A member of the FGF family whose expression is dependent on Sonic hedgehog signaling
14	ASS1	8.813	445	Argininosuccinate synthetase 1	The enzyme that catalyzes the penultimate step of the arginine biosynthetic pathway
15	S100A4	8.555	6275	S100 calcium binding protein A4	A member of the S100 family of proteins involved in motility, invasion, and tubulin polymerization
16	LIX1	7.99	167410	Lix1 homolog (chicken)	A protein involved in RNA metabolism that has an essential function for motor neuron survival
17	FAM65B	7.974	9750	Family with sequence similarity 65, member B	a protein involved in myogenic cell differentiation
18	NOG	7.65	9241	Noggin	A secreted protein that plays a principal role in creating morphogenic gradients by antagonizing bone morphogenetic proteins
19	C1orf115	7.571	79762	Chromosome 1 open reading frame 115	An integral membrane protein of unknown function
20	CYSLTR2	7.23	57105	Cysteinyl leukotriene receptor 2	A G protein-coupled receptor for cysteinyl leukotrienes

Genome-wide gene expression profiling of F3-WT and F3-Ngn1 was performed by using two sets of Human Gene 1.0 ST Array for each, followed by two comparisons composed of WT array-1 (F3-WT-1) versus Ngn1 array-1 (F3-Ngn1-1) and WT array-2 (F3-WT-2) versus Ngn1 array-2 (F3-Ngn1-2). Top 20 upregulated genes in F3-Ngn1 cells are shown with fold change derived from the comparison between F3-WT-2 and F3-Ngn1-2

genes directly linked to the 537 genes. Subsequently, we performed the "N-points to N-points" search by starting from Ngn1 and ending with the set of 787 genes via the shortest route connecting starting and ending points. It generated a highly complex molecular network composed of 1,816 fundamental nodes and 7,238 molecular relations (Fig. 6). When the network was referred to the canonical pathways of the KeyMolnet library, the generated network has the most significant relationship with transcriptional regulation by nuclear factor kappa-B (NF-κB) with the score of 59.9 and score (p) = 9.467E−019. This was followed by transcriptional regulation by cyclic AMP-response element-binding protein (CREB) in the second rank with the score of 52.3 and score (p) = 1.771E−016, transcriptional regulation by vitamin D receptor (VDR) in the third rank with the score of 45.8 and score (p) = 1.582E−014, transcriptional

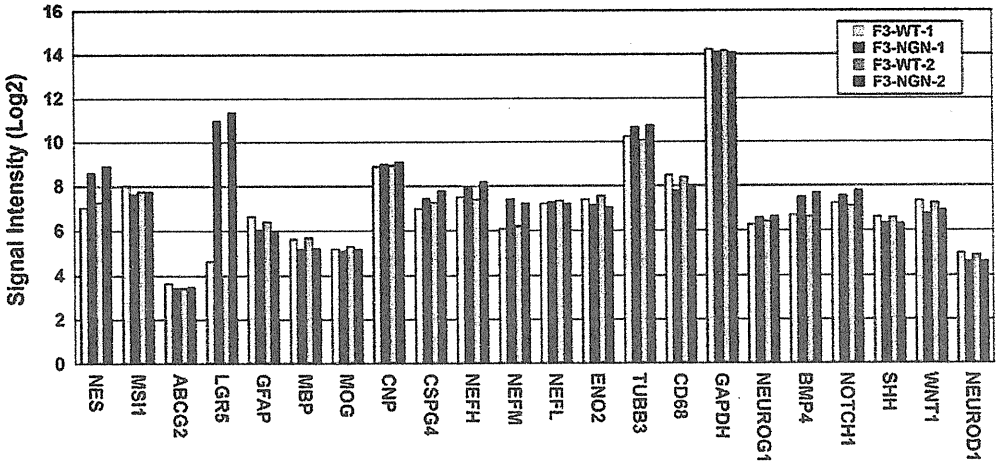

Fig. 3 Gene expression profiles of NSC, neuronal and glial markers. Genome-wide gene expression profiling of F3-WT and F3-Ngn1 was performed by using two sets of Human Gene 1.0 ST Array for each, followed by two comparisons composed of WT array-1 (F3-WT-1; the first column) versus Ngn1 array-1 (F3-Ngn1-1; the second column) and WT array-2 (F3-WT-2; the third column) versus Ngn1 array-2 (F3-Ngn1-2; the fourth column). Signal intensities of NSC, neuronal and glial marker genes are expressed as log 2 after normalization. *NES* nestin, *MSI1* musashi homolog 1, *ABCG2* ATP-binding cassette, subfamily G member 2, *LGR5* leucine-rich repeat-containing G protein-coupled receptor 5, *GFAP* glial fibrillary acidic protein, *MBP* myelin basic protein, *MOG* myelin oligodendrocyte glycoprotein, *CNP*, 2′3′-cyclic nucleotide 3′ phosphodiesterase, *CSPG4* chondroitin sulfate proteoglycan 4 (NG2), *NEFH* neurofilament heavy polypeptide, *NEFM* neurofilament medium polypeptide, *NEFL* neurofilament light polypeptide, *ENO2* enolase 2 (NSE), *TUBB3* tubulin beta 3, *GAPDH* glyceraldehyde-3-phosphate dehydrogenase (G3PDH), *NEUROG1* neurogenin 1, *BMP4* bone morphogenic protein 4, *NOTCH1* notch homolog 1, *SHH* sonic hedgehog homolog, *WNT1* wingless-type MMTV integration site family member 1, and *NEUROD1* neurogenic differentiation 1. A robust upregulation of LGR5 is evident in both F3-Ngn1-1 and F3-Ngn1-2

regulation by hypoxia-inducible factor (HIF) in the fourth rank with the score of 35.7 and score (p) = 1.781E−011, transcriptional regulation by glucocorticoid receptor (GR) in the fifth rank with the score of 31.0 and score (p) = 4.779E−010, and the complement activation pathway in the sixth rank with the score of 20.5 and score (p) = 6.589E−007. Thus, the molecular network of the genes differentially expressed between F3-WT and F3-Ngn1 involves the complex interaction of networks regulated by multiple transcription factors.

Gene Annotation Analysis Suggested Multifunctional Changes in F3-Ngn1 Cells

We studied functional annotation terms overrepresented in 588 DEG by using the web-accessible program named DAVID. By importing the list of Entrez Gene ID, DAVID identified top 20 enriched gene ontology (GO) terms in the list of 250 upregulated genes, most of which are related to development and morphogenesis (Table 4). In contrast, top 20 enriched GO terms in the list of 338 downregulated genes were chiefly composed of the molecules closely associated with extracellular matrix and adhesion (Table 4). Thus, gene annotation analysis suggested that stable expression of a single gene Ngn1 in F3 cells induces multifunctional changes that potentially affect the differentiation of human NSC.

Discussion

Recently, we established an immortalized human NSC clone named HB1.F3, which could serve as an unlimited source for cell replacement therapy of various neurological diseases (Kim 2004; Kim and de Vellis 2009). Ngn1 is a proneural bHLH transcription factor that promotes neuronal differentiation but inhibits glial differentiation of rodent NSC and NPC (Morrison 2001; Sun et al. 2001). In the present study, to investigate a role of Ngn1 in human NSC differentiation, we established a clone derived from F3 stably overexpressing Ngn1. Genome-wide gene expression profiling identified 250 upregulated genes and 338 downregulated genes in F3-Ngn1 versus F3-WT cells. Notably, the expression of LGR5, a recently identified marker for intestine and hair follicle stem cells (Barker et al. 2007; Jaks et al. 2008; Sato et al. 2009), was greatly elevated in F3-Ngn1 cells at both mRNA and protein levels. However, transient overexpression of Ngn1 did not induce upregulation of LGR5 in F3-WT cells, suggesting that LGR5 is not a direct transcriptional target of Ngn1. KeyMolnet, a bioinformatics tool for analyzing molecular relations on a comprehensive knowledgebase, indicated that the molecular network of differentially expressed genes involves the complex interaction of networks regulated by multiple transcription factors, such as NF-κB, CREB, VDR, HIF, and GR. Gene annotation analysis

Table 3 Top 20 downregulated genes in F3 cells following stable expression of neurogenin 1

No.	Gene symbol	Fold change	Entrez gene ID	Gene name	Putative function
1	HAS2	0.024	3037	Hyaluronan synthase 2	The enzyme involved in synthesis and transport of hyaluronic acid
2	MMP9	0.044	4318	Matrix metallopeptidase 9 (gelatinase B, 92 kDa gelatinase, 92 kDa type IV collagenase)	The enzyme that degrades type IV and V collagens involved in embryonic development and tissue remodeling
3	C3	0.05	718	Complement component 3	A protein that plays a central role in the activation of complement system
4	LCP1	0.05	3936	Lymphocyte cytosolic protein 1 (L-plastin)	An actin-binding protein that plays a role in cell adhesion-dependent signaling
5	PAPPA	0.068	5069	Pregnancy-associated plasma protein A, pappalysin 1	A secreted metalloproteinase which cleaves insulin-like growth factor binding proteins
6	DSP	0.072	1832	Desmoplakin	A component of functional desmosomes that anchors intermediate filaments to desmosomal plaques
7	SPOCK1	0.075	6695	Sparc/osteonectin, cwcv and kazal-like domains proteoglycan (testican) 1	A chondroitin sulfate/heparan sulfate proteoglycan expressed in the postsynaptic region of hippocampal pyramidal neurons
8	TRIM22	0.076	10346	Tripartite motif-containing 22	A member of the tripartite motif family induced by interferon and mediates interferon's antiviral effects
9	CCND2	0.087	894	Cyclin D2	A protein that forms a complex with CDK kinases involved in cell cycle G1/S transition
10	IL6	0.088	3569	Interleukin 6 (interferon, beta 2)	An immunoregulatory cytokine that functions in inflammation and the maturation of B cells
11	CD82	0.092	3732	CD82 molecule	A membrane glycoprotein activated by p53 involved in suppression of metastasis
12	SLC43A3	0.093	29015	Solute carrier family 43, member 3	An integral membrane protein of the SLC43A transporter family
13	GREM1	0.093	26585	Gremlin 1, cysteine knot superfamily, homolog (*Xenopus laevis*)	A member of bone morphogenic protein antagonist family expressed in the neural crest
14	INHBA	0.095	3624	Inhibin, beta A	A growth/differentiation factor for various cell types by acting as a homodimer (activin A) or a heterodimer (activin A-B)
15	ITGB3	0.095	3690	Integrin, beta 3 (platelet glycoprotein IIIa, antigen CD61)	A subunit of integrins involved in cell adhesion and cell-surface-mediated signaling
16	FAP	0.097	2191	Fibroblast activation protein, alpha	A homodimeric integral membrane gelatinase involved in epithelial–mesenchymal interactions during development
17	C1S	0.101	716	Complement component 1, s subcomponent	A major constituent of the human complement subcomponent C1 that associates with C1r and C1q to yield the first component of the serum complement system
18	PXDN	0.103	7837	Peroxidasin homolog (Drosophila)	An extracellular matrix-associated peroxidase involved in extracellular matrix consolidation
19	C4orf18	0.103	51313	Chromosome 4 open reading frame 18	A Golgi apparatus membrane of unknown function
20	CFH	0.104	3075	Complement factor H	Q serum glycoprotein that regulates the function of the alternative complement pathway

Genome-wide gene expression profiling of F3-WT and F3-Ngn1 was performed by using two sets of Human Gene 1.0 ST Array for each, followed by two comparisons composed of WT array-1 (F3-WT-1) versus Ngn1 array-1 (F3-Ngn1-1) and WT array-2 (F3-WT-2) versus Ngn1 array-2 (F3-Ngn1-2). Top 20 downregulated genes in F3-Ngn1 cells are shown with fold change derived from the comparison between F3-WT-2 and F3-Ngn1-2

suggested that GO terms of development and morphogenesis are enriched in upregulated genes, while those of extracellular matrix and adhesion are enriched in downregulated genes. These results suggest that stable expression of a single gene Ngn1 in F3 cells induces not simply neurogenic but multifunctional changes that potentially affect the differentiation of human NSC via a reorganization of complex gene regulatory networks.

LGR5, an orphan G protein-coupled receptor alternatively named GRP49 with structural similarity to the

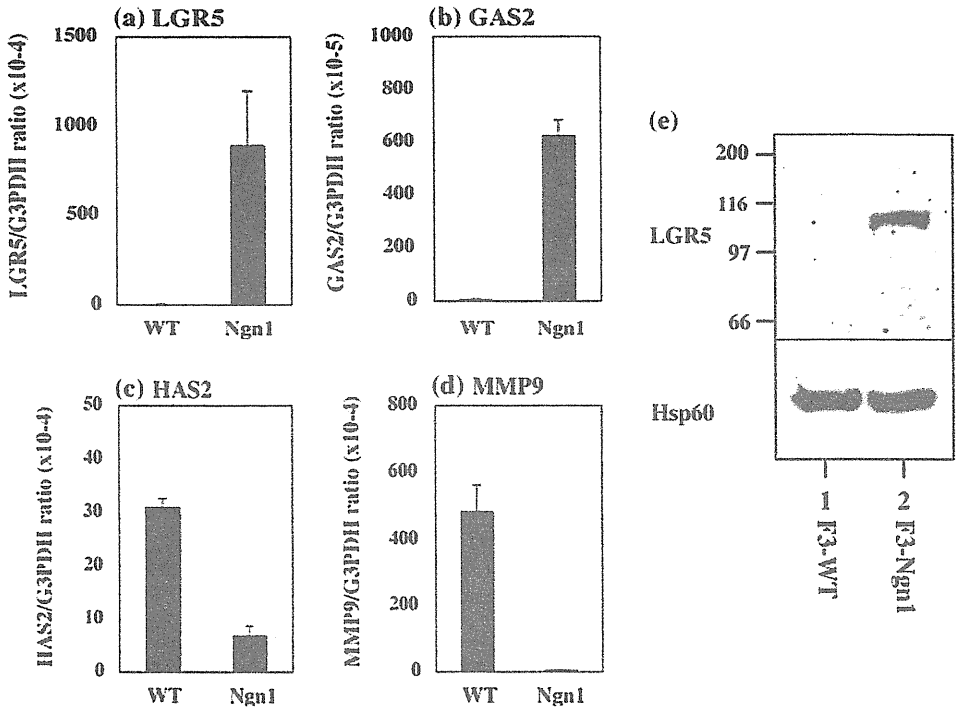

Fig. 4 Real-time RT-PCR and Western blot analysis. cDNA prepared from F3-WT and F3-Ngn1 cells was processed for real-time RT-PCR using primer sets listed in Table 1. Total protein extract was processed for western blot with anti-LGR5 antibody. The panels (a–e) represent real-time RT-PCR of a LGR5, b GAS2, c HAS2, and d MMP9, and western blot of (e, *upper panel*) LGR5 and (e, *lower panel*) Hsp60, an internal control for protein loading

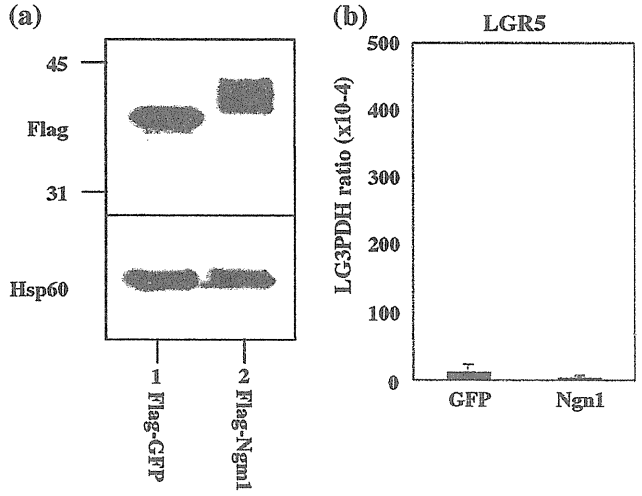

Fig. 5 Transient overexpression of Ngn1 did not induce upregulation of LGR5 in F3-WT cells. Expression vectors of Flag-tagged Ngn1 or GFP were transfected in F3-WT cells. At 48 h after transfection, the cells were processed for Western blot analysis of Flag and real-time RT-PCR analysis of LGR5. a Western blot analysis. The lanes (1, 2) represent *1* Flag-tagged GFP and *2* Flag-tagged Ngn1. The *upper panel* indicates Flag-tagged proteins, while the *lower panel* indicates Hsp60, an internal control for protein loading. b Real-time RT-PCR analysis. The *left bar* represents F3-WT cells with transient overexpression of Flag-tagged GFP, while the *right bar* represents those with transient overexpression of Flag-tagged Ngn1

glycoprotein hormone receptor family, is recently identified as a marker of adult intestinal stem cells and hair follicle stem cells by lineage-tracing studies (Barker et al. 2007; Jaks et al. 2008; Sato et al. 2009). LGR5 expression is also identified in the adult human spinal cord and brain at least at mRNA levels (Hsu et al. 1998). At present, the precise physiological function of LGR5 and downstream signaling pathways remain unknown owing to the lack of an identified natural ligand. LGR gene knockout mice showed neonatal lethality due to a breast-feeding defect caused by ankyloglossia, suggesting an involvement of LGR5 in craniofacial development (Morita et al. 2004). A more recent study showed that LGR5 deficiency induces premature differentiation of Paneth cells in the small intestine, accompanied by overactivation of the Wnt pathway, indicating that LGR5 acts as a negative regulator of Wnt (Garcia et al. 2009). A different study revealed that LGR5 is a marker for the sublineage of intestinal stem cells that are responsive to Wnt signals derived from stem cell niche (Ootani et al. 2009). In the populations of intestinal stem cells, LGR5 labels cycling cells, while doublecortin-like kinase-1 (DCLK1) marks quiescent cells (May et al. 2009). Interestingly, the expression of DCLK2, a putative paralog of DCLK1, is elevated with a 3.38-fold increase in F3-Ngn1 cells (Supplementary Table 1).

The interaction between Wnt proteins and Frizzled receptors on the cell surface transduces the signals to β-catenin by inactivating glycogen synthase kinase 3β (GSK3β), and stabilized β-catenin is translocated into the nucleus and forms a complex with T-cell factor (TCF) transcription factors to activate transcription of Wnt target genes. Importantly, LGR5 is identified as one of Wnt target genes (Yamamoto et al. 2003), suggesting a key role of LGR5 in establishment of a negative feedback loop in the